RICE UNIVERSITY

Studies of one- and two-photon photoassociative spectroscopy using ultracold strontium

by

James Allen Aman

A Thesis Submitted
in Partial Fulfillment of the
Requirements for the Degree

Doctor of Philosophy

Approved, Thesis Committee:

Thomas C. Killian, Chair
Professor of Physics and Astronomy

Randall G. Hulet
Fayez Sarofim Professor of Physics and Astronomy

Kevin F. Kelly
Associate Professor of Electrical and Computer Engineering

Houston, Texas

April, 2019

ABSTRACT

Studies of one- and two-photon photoassociative spectroscopy using ultracold strontium

by

James Allen Aman

"Lorem ipsum dolor sit amet, consectetur adipiscing elit, sed do eiusmod tempor incididunt ut labore et dolore magna aliqua. Ut enim ad minim veniam, quis nostrud exercitation ullamco laboris nisi ut aliquip ex ea commodo consequat. Duis aute irure dolor in reprehenderit in voluptate velit esse cillum dolore eu fugiat nulla pariatur. Excepteur sint occaecat cupidatat non proident, sunt in culpa qui officia deserunt mollit anim id est laborum."

Acknowledgments

"Lorem ipsum dolor sit amet, consectetur adipiscing elit, sed do eiusmod tempor incididunt ut labore et dolore magna aliqua. Ut enim ad minim veniam, quis nostrud exercitation ullamco laboris nisi ut aliquip ex ea commodo consequat. Duis aute irure dolor in reprehenderit in voluptate velit esse cillum dolore eu fugiat nulla pariatur. Excepteur sint occaecat cupidatat non proident, sunt in culpa qui officia deserunt mollit anim id est laborum."

Contents

Illustrations

Tables

Chapter 1

Introduction

"Lorem ipsum dolor sit amet, consectetur adipiscing elit, sed do eiusmod tempor incididunt ut labore et dolore magna aliqua. Ut enim ad minim veniam, quis nostrud exercitation ullamco laboris nisi ut aliquip ex ea commodo consequat. Duis aute irure dolor in reprehenderit in voluptate velit esse cillum dolore eu fugiat nulla pariatur. Excepteur sint occaecat cupidatat non proident, sunt in culpa qui officia deserunt mollit anim id est laborum."

Should probably mention somewhere that this is long-range PA, in contrast to short-range stuff being explored now.

[1]

1.1 Few-body physics

"Lorem ipsum dolor sit amet, consectetur adipiscing elit, sed do eiusmod tempor incididunt ut labore et dolore magna aliqua. Ut enim ad minim veniam, quis nostrud exercitation ullamco laboris nisi ut aliquip ex ea commodo consequat. Duis aute irure dolor in reprehenderit in voluptate velit esse cillum dolore eu fugiat nulla pariatur. Excepteur sint occaecat cupidatat non proident, sunt in culpa qui officia deserunt mollit anim id est laborum."

1.2 Halo molecules

"Lorem ipsum dolor sit amet, consectetur adipiscing elit, sed do eiusmod tempor incididunt ut labore et dolore magna aliqua. Ut enim ad minim veniam, quis nostrud exercitation ullamco laboris nisi ut aliquip ex ea commodo consequat. Duis aute irure dolor in reprehenderit in voluptate velit esse cillum dolore eu fugiat nulla pariatur. Excepteur sint occaecat cupidatat non proident, sunt in culpa qui officia deserunt mollit anim id est laborum."

1.3 Properties of strontium

"Lorem ipsum dolor sit amet, consectetur adipiscing elit, sed do eiusmod tempor incididunt ut labore et dolore magna aliqua. Ut enim ad minim veniam, quis nostrud exercitation ullamco laboris nisi ut aliquip ex ea commodo consequat. Duis aute irure dolor in reprehenderit in voluptate velit esse cillum dolore eu fugiat nulla pariatur. Excepteur sint occaecat cupidatat non proident, sunt in culpa qui officia deserunt mollit anim id est laborum."

1.4 Thesis Outline

"Lorem ipsum dolor sit amet, consectetur adipiscing elit, sed do eiusmod tempor incididunt ut labore et dolore magna aliqua. Ut enim ad minim veniam, quis nostrud exercitation ullamco laboris nisi ut aliquip ex ea commodo consequat. Duis aute irure dolor in reprehenderit in voluptate velit esse cillum dolore eu fugiat nulla pariatur. Excepteur sint occaecat cupidatat non proident, sunt in culpa qui officia deserunt mollit anim id est laborum."

Natural Abundances (%)		Scattering Lengths (a_0)			
		^{84}Sr	^{86}Sr	^{87}Sr	^{88}Sr
0.56	^{84}Sr	122.76	31.65	-57.61	1658
9.86	^{86}Sr	~	798	162.25	97.37
7.00	^{87}Sr	~	~	96.2	54.82
82.58	^{88}Sr	~	~	~	-2

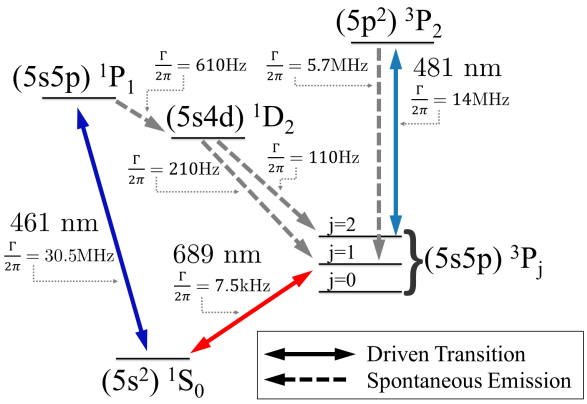

Figure 1.1 : Properties of strontium

Properties of strontium. Left: Natural abundances and s-wave scattering lengths for all mixtures of Sr. Right: Simplified energy level diagram of Sr showing the relevant states used for trapping and cooling of the atomic gas

$$V(x) = V_{lat}\ \sin^2(k_L x) \tag{1.1}$$

Chapter 2

The Neutral apparatus

"Lorem ipsum dolor sit amet, consectetur adipiscing elit, sed do eiusmod tempor incididunt ut labore et dolore magna aliqua. Ut enim ad minim veniam, quis nostrud exercitation ullamco laboris nisi ut aliquip ex ea commodo consequat. Duis aute irure dolor in reprehenderit in voluptate velit esse cillum dolore eu fugiat nulla pariatur. Excepteur sint occaecat cupidatat non proident, sunt in culpa qui officia deserunt mollit anim id est laborum."

2.1 Vacuum system

"Lorem ipsum dolor sit amet, consectetur adipiscing elit, sed do eiusmod tempor incididunt ut labore et dolore magna aliqua. Ut enim ad minim veniam, quis nostrud exercitation ullamco laboris nisi ut aliquip ex ea commodo consequat. Duis aute irure dolor in reprehenderit in voluptate velit esse cillum dolore eu fugiat nulla pariatur. Excepteur sint occaecat cupidatat non proident, sunt in culpa qui officia deserunt mollit anim id est laborum."

2.2 Laser systems

"Lorem ipsum dolor sit amet, consectetur adipiscing elit, sed do eiusmod tempor incididunt ut labore et dolore magna aliqua. Ut enim ad minim veniam, quis nostrud

exercitation ullamco laboris nisi ut aliquip ex ea commodo consequat. Duis aute irure dolor in reprehenderit in voluptate velit esse cillum dolore eu fugiat nulla pariatur. Excepteur sint occaecat cupidatat non proident, sunt in culpa qui officia deserunt mollit anim id est laborum."

2.2.1 Wideband cooling stage: 461 nm

"Lorem ipsum dolor sit amet, consectetur adipiscing elit, sed do eiusmod tempor incididunt ut labore et dolore magna aliqua. Ut enim ad minim veniam, quis nostrud exercitation ullamco laboris nisi ut aliquip ex ea commodo consequat. Duis aute irure dolor in reprehenderit in voluptate velit esse cillum dolore eu fugiat nulla pariatur. Excepteur sint occaecat cupidatat non proident, sunt in culpa qui officia deserunt mollit anim id est laborum."

2.2.2 Narrowband cooling stage: 689 nm

"Lorem ipsum dolor sit amet, consectetur adipiscing elit, sed do eiusmod tempor incididunt ut labore et dolore magna aliqua. Ut enim ad minim veniam, quis nostrud exercitation ullamco laboris nisi ut aliquip ex ea commodo consequat. Duis aute irure dolor in reprehenderit in voluptate velit esse cillum dolore eu fugiat nulla pariatur. Excepteur sint occaecat cupidatat non proident, sunt in culpa qui officia deserunt mollit anim id est laborum."

2.2.3 Repumping: 481 nm

"Lorem ipsum dolor sit amet, consectetur adipiscing elit, sed do eiusmod tempor incididunt ut labore et dolore magna aliqua. Ut enim ad minim veniam, quis nostrud

exercitation ullamco laboris nisi ut aliquip ex ea commodo consequat. Duis aute irure dolor in reprehenderit in voluptate velit esse cillum dolore eu fugiat nulla pariatur. Excepteur sint occaecat cupidatat non proident, sunt in culpa qui officia deserunt mollit anim id est laborum."

2.2.4 Optical dipole trap: 1064 nm

Discuss how our only method for evaporative cooling is through light traps since we do not have a magnetically sensitive ground state.

2.2.5 Optical toolbox

"Lorem ipsum dolor sit amet, consectetur adipiscing elit, sed do eiusmod tempor incididunt ut labore et dolore magna aliqua. Ut enim ad minim veniam, quis nostrud exercitation ullamco laboris nisi ut aliquip ex ea commodo consequat. Duis aute irure dolor in reprehenderit in voluptate velit esse cillum dolore eu fugiat nulla pariatur. Excepteur sint occaecat cupidatat non proident, sunt in culpa qui officia deserunt mollit anim id est laborum."

2.3 Electronics

"Lorem ipsum dolor sit amet, consectetur adipiscing elit, sed do eiusmod tempor incididunt ut labore et dolore magna aliqua. Ut enim ad minim veniam, quis nostrud exercitation ullamco laboris nisi ut aliquip ex ea commodo consequat. Duis aute irure dolor in reprehenderit in voluptate velit esse cillum dolore eu fugiat nulla pariatur. Excepteur sint occaecat cupidatat non proident, sunt in culpa qui officia deserunt mollit anim id est laborum."

2.3.1 Computer control system

"Lorem ipsum dolor sit amet, consectetur adipiscing elit, sed do eiusmod tempor incididunt ut labore et dolore magna aliqua. Ut enim ad minim veniam, quis nostrud exercitation ullamco laboris nisi ut aliquip ex ea commodo consequat. Duis aute irure dolor in reprehenderit in voluptate velit esse cillum dolore eu fugiat nulla pariatur. Excepteur sint occaecat cupidatat non proident, sunt in culpa qui officia deserunt mollit anim id est laborum."

2.3.2 Standalone systems

"Lorem ipsum dolor sit amet, consectetur adipiscing elit, sed do eiusmod tempor incididunt ut labore et dolore magna aliqua. Ut enim ad minim veniam, quis nostrud exercitation ullamco laboris nisi ut aliquip ex ea commodo consequat. Duis aute irure dolor in reprehenderit in voluptate velit esse cillum dolore eu fugiat nulla pariatur. Excepteur sint occaecat cupidatat non proident, sunt in culpa qui officia deserunt mollit anim id est laborum."

2.4 Apparatus benchmarks

"Lorem ipsum dolor sit amet, consectetur adipiscing elit, sed do eiusmod tempor incididunt ut labore et dolore magna aliqua. Ut enim ad minim veniam, quis nostrud exercitation ullamco laboris nisi ut aliquip ex ea commodo consequat. Duis aute irure dolor in reprehenderit in voluptate velit esse cillum dolore eu fugiat nulla pariatur. Excepteur sint occaecat cupidatat non proident, sunt in culpa qui officia deserunt mollit anim id est laborum."

Chapter 3

Photoassociation spectroscopy: theory and methods

3.1 Introduction

This part needs to be brief and really should motivate the idea of PAS.

Okk, first ogg we introduce the potential between atoms

this arises from the interaction of scattering theory with a molecular state. "the interaction potential between two atoms. Ehich is caused by?

this results in a poitential that supports bound states . In atomic physics, our low density fases are mainly within the regime of small interactions. This spatial dependence is mapped onto the internal energy levels of each atom. I want to say dressed state model here (review atom-photon coupling, atomic physics book).

Definitely need some BS about how simple scattering theory has been a hallmark of atomic physics and

What about the history of scattering? Most of what we know about quantum mechanics comes from either scattering experiments of spectroscopy. Photoassociation spectroscopy is an important field which relies on both of these properties.

3.1.1 PAS in atomic physics

PA is not unique to atomic physics, chemists have been using light to interrogate molecular structure for a long time

physicists molecule, short-range PA, rabi oscilations between atomic and molecular condensates (cite ours and the lattice experiment that followed)

Pioneering work done in the early 90's used PA to interrogate the sturucture of interatomic potentials to deduce the scattering lengths between atoms.

Can even be used to modify the scattering length of atoms through mixing of atomic eigenstates.

This work is focused on long-range PA but in recent years groups have also developed short-range PA techniques for the creation of ro-vibrational ground state molecules. These techniques rely heavily on favorable overlap integrals betwwen molecular wavefunctions and typically searching for favorable intermediate states is a pain (that is why our large FCF might be useful)

There are multiple flavors of PAS. Can do one-photon or two-photon.

3.1.2 Low energy two-body scattering

consider the two particle system as a single entagled particle long range part of this quasi-particle is just the eigenstates of the separate particles themselves (only composed of two parts) but the short range part is going to be determined by some complex physics (new eigenstates, what is the coupling mechanism?) the vdW point is the boundary distance? coupling is due to the interatomic potential, there is at

least the long-range part falling off as R6, what are the types of interactions which make up the internal wall?

Think I want to introduce the photoassocation by talking about the collisional wavefunction

what will that do?

I want to build up ideas about the FCF and need the wf for that to get qf I have to go back to scattering theory

ideas of the wavefunction become that basis for how you want to talk about interacting potentials

free atoms scatering as single particle state (differnet eigenstate) interaction determined by some gnarly stuff From scattering theory we know that the long range behavior is determined by short range physics how do we know this? (the dalibard intro) Can we come up with good enough pseudo potentials to describe the short range physics and then solve the schrodinger equation to extract wavefunctions? we want wavefunctions because that is the full characterization we don't know the right eigenbasis for the short range part but we can make some guesses (in particular Hund cases setup eigen states for various possible internal states) Bohn and Julienne theory guessed based on using quantum defect theory this pre-supposes that the bound and free wavefunctions are similar (I forget in what respect) but that the bound ones must go to zero as R-¿Inf If we have some notion of the wf then we can construct matricies which define interactions once we add additional coupling to the scattering problem

now in a position where I need to connect scattering theory and the PAS

Natural Abundances (%)		Scattering Lengths (a_0)			
		^{84}Sr	^{86}Sr	^{87}Sr	^{88}Sr
0.56	^{84}Sr	122.76	31.65	-57.61	1658
9.86	^{86}Sr	~	798	162.25	97.37
7.00	^{87}Sr	~	~	96.2	54.82
82.58	^{88}Sr	~	~	~	-2

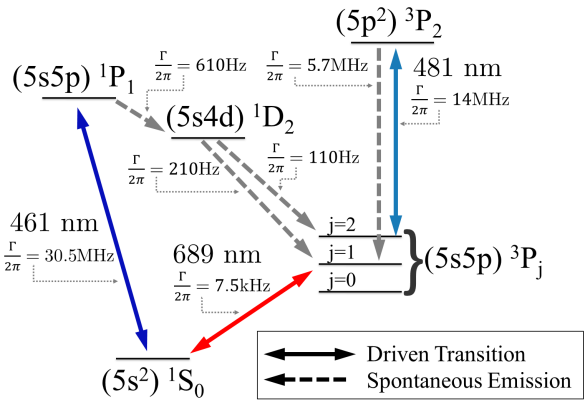

Figure 3.1 : Strontium interatomic wavefunctions

Res 6.3

Once we have the ground state wavefunction of our new particle we can construct the internal structure by considering the internal energy strucutrue of the constituent atoms Can I make a connnection that since it is a composite particle we must consider all the various configurations available?

3.1.3 Modifying interactions

Also the Chin '10 review on feshbach resonances

Follow the Nicholson 15 paper method of introing the elastic and inelastic cross sections

3.2 Semi-classical treatment of lineshapes

Now that we have the theory of PAS covered. PA can come in many forms (in a lattice, in a bulk gas, via dissociating molecules) Experimentally we observe PA by looking for trap loss doublon paper.

This section will cover the theory of lineshapes in PAS.

Somewhere I read about three regimes of PAS as a comparison of relevant energy scales. Should explore that here

$$N(t) = \frac{N_0 \mathrm{e}^{-\Gamma \mathrm{t}}}{1 + \frac{2\mathrm{N_0}\langle \mathrm{K} \rangle \mathrm{V_2}}{\Gamma \mathrm{V_1^2}}(1 - \mathrm{e}^{-\Gamma \mathrm{t}})} \tag{3.1}$$

where N_0 is the number at the beginning of the PAS interaction time, and $\langle K \rangle$ indicates a spatial average of collision event rate constant K (Eq. 4.4). The one-body loss rate, Γ, is due to background collisions and off-resonant scattering from the PA lasers.

PA loss is described with a local equation for the evolution of the atomic density [Eq. (4.1)]. Integrating Eq. (4.1) over the trap volume yields the time evolution of the number of trapped atoms [Eq. (4.2)]. The effective volumes used throughout this analysis are defined by

$$V_{\mathrm{q}} = \int_{\mathrm{V}} d^3 r \, e^{-\frac{qU(\mathbf{r})}{k_B T}}, \tag{3.2}$$

for trapping potential $U(\mathbf{r})$. The collision event rate constant can be expressed as a thermal average of the scattering probability for loss, $|S(\epsilon, \omega_1, \omega_2, ..., \mathbf{r})|^2$, over the collision energy ϵ. We also average over the trap volume to allow for the possibility that the scattering probability can vary with position in the trap due to inhomogeneity of laser intensity profiles and the density distribution [Eq. (4.4)].

$$\langle K\rangle = \frac{1}{V_2}\int_{\mathrm{V}} d^3r\, e^{-\frac{2U(\mathbf{r})}{k_BT}} \times\frac{1}{h\,Q_T}\int_0^{U_{max}-U(r)} d\epsilon|S|^2\, e^{-\epsilon/k_BT}. \tag{3.3}$$

where the partition function is $Q_T = \left(\frac{2\pi k_B T\mu}{h^2}\right)^{3/2}$ for reduced mass μ.

Bohn and Julienne [**?**] provide an expression for $|S(\epsilon,\omega_1,\omega_2,...)|^2$ for a collision on the open channel of two ground state atoms (g) with total energy ϵ leading to loss-producing decay from the excited state b_1 with rate γ_1. (See Fig. 4.1.) It yields

$$|S|^2 = \frac{(\Delta_2+\epsilon/\hbar)^2\gamma_1\gamma_s}{\left[(\Delta_1+\epsilon/\hbar)(\Delta_2+\epsilon/\hbar)-\frac{\Omega_{12}^2}{4}\right]^2+\left[\frac{\gamma_1+\gamma_s}{2}\right]^2(\Delta_2+\epsilon/\hbar)^2}, \tag{3.4}$$

where all quantities are defined in the main text. For simplicity, we have omitted the light shift of b_1 due to coupling to the scattering continuum [**?**]. Equation (4.5) neglects all light shifts due to the trapping laser. Light shifts due to the photoassociation lasers coupling to states outside our model (Fig. 4.1) are also neglected. The thermal energy is much greater than the zero-point energy for trap motion, $T \gg h\nu_{\mathrm{trap}}/k_B$, so confinement effects are negligible [**?**].

and lights shifts of states 0 and 2 are approximately equal and will cancel in the determination of the binding energy of the halo state, E_2 [**?** 2]. Neglecting

For the experiments reported here, we maintain significant intermediate-state detuning, $|\Delta_1| \gg |\Omega_{12}|$. Thus we are in a Raman configuration, and near two-photon resonance the expression for the scattering probability for a given initial scattering

energy Eq. (4.5) can be approximated as a Lorentzian

$$|S|^2 \approx \frac{A(\epsilon)}{\left(\Delta_2 + \epsilon/\hbar - \frac{\Omega_{12}^2}{4(\Delta_1+\epsilon/\hbar)}\right)^2 + \left[\Gamma_L(\epsilon)/2\right]^2}, \tag{3.5}$$

where A and Γ_L are defined in Eqs. (4.8) and (4.9).

As discussed in the text, we analyze loss spectra using the effective expression, Eq. (4.10) to account for possible deviations from the single-channel theory [**?**].

The total 689-nm intensity oscillates with 100% contrast according to $I_{total} = I_1 + I_2 + 2\sqrt{I_1 I_2}\cos\left[(\omega_1 - \omega_2)t\right] = 2I\left\{1 + \cos\left[(\omega_1 - \omega_2)t\right]\right\}$. Equation 4.16 The form of the AC Stark shift due to excitation lasers in Eq. 4.11 reflects the time average of the intensity and neglects the interference term. To confirm that this is the correct description, we numerically solved the time-evolution for a three-level system with similar optical couplings and oscillating optical intensity as present during halo photoassociation. The Hamiltonian is

$$H = \tag{3.6}$$

$$\begin{pmatrix} 0 & \Omega_{01}\left[\cos(\omega_1 t) + \cos(\omega_2 t)\right] & 0 \\ . & E_{b1} & \Omega_{12}\left[\cos(\omega_1 t) + \cos(\omega_2 t)\right] \\ . & . & E_{b2} \end{pmatrix}$$

For $\Omega_{01} \ll \Omega_{12} \ll \Delta_1 \equiv E_{b1}/\hbar - \omega_1$, which is analogous to the experimental conditions used here

, the shift of the two-photon resonance condition follows $\delta = \Omega_{12}^2/2\Delta_1$ in agreement with Eq. 4.16.

Natural Abundances (%)		Scattering Lengths (a_0)			
		^{84}Sr	^{86}Sr	^{87}Sr	^{88}Sr
0.56	^{84}Sr	122.76	31.65	-57.61	1658
9.86	^{86}Sr	~	798	162.25	97.37
7.00	^{87}Sr	~	~	96.2	54.82
82.58	^{88}Sr	~	~	~	-2

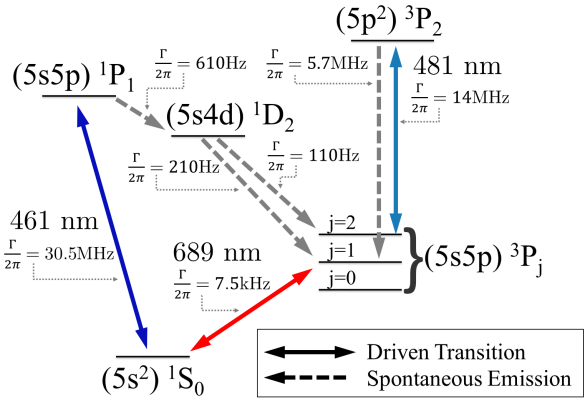

Figure 3.2 : Strontium two-photon photoassociation

fig 1 from the halo paper

3.3 Observing photoassociative loss

In this work, we probe the halo state in 86Sr using two-photon Raman photoassociation (PA) cite 16 from halo paper, in which two laser fields couple colliding atoms to the least-bound state of the ground molecular potential. We tune near resonance with an intermediate state that is bound in the 0u potential corresponding to the $^1S_0 + {}^3P_1$ asymptote at long range as shown in Fig.3.3.

Photoassociation experiments follow the same general presciprtion. We start by trapping through the normal sequence as outlined in some section. Then we evaporate down to the final trap depth. After evaporation

The two-photon PAS experiments described in the following chapters are performed under similar conditions but due to complications with the neutral vaccuum system we performed the binding energy experiemtns using the Rydberg apparatus. While non-ideal from a consistency point of view, this did allow us to replicate and

validate our previous findings which gives us great confidence in the robustness of this experimental appraoch.

The most significant difference between the two apparatus' is the trapping characteristics of the optical dipole traps and the beam parameters of the photoassociation beam. These differences are noted in the corresponding chapters but here we will outline the timing and generic characteristics that are shared between the two experiments.

Table something shows the relevant experimental parameters and typical values for our photoassociation experiments.

Specific details of the optical dipole traps, PA beam parameters, and using a completely different a

performed on ultracold Sr atoms in a single-beam optical dipole trap (ODT) generated from a 1064-nm laser propagating perpendicular to gravity. Typical atom numbers are several hundred thousand and peak densities are $\approx n_0 = 1 \times 10^{12}\,\mathrm{cm}^{-3}$. The number of atoms and sample temperature are measured using time-of-flight absorption imaging described in some section. Trap oscillation frequencies are determined by measuring dipole and breathing collective mode frequencies, which allow determination of trap volume and sample density

For experiments done on our apparatus we generate the two photon source as shown in Fig**??**. Light comes from an injection locked slave diode which follows the frequency stablized 689 master laser described in some section. THis light is modulated via a single acousto-optic modulator (AOM) driven with two frequencies

Natural Abundances (%)		Scattering Lengths (a_0)			
		^{84}Sr	^{86}Sr	^{87}Sr	^{88}Sr
0.56	^{84}Sr	122.76	31.65	-57.61	1658
9.86	^{86}Sr	~	798	162.25	97.37
7.00	^{87}Sr	~	~	96.2	54.82
82.58	^{88}Sr	~	~	~	-2

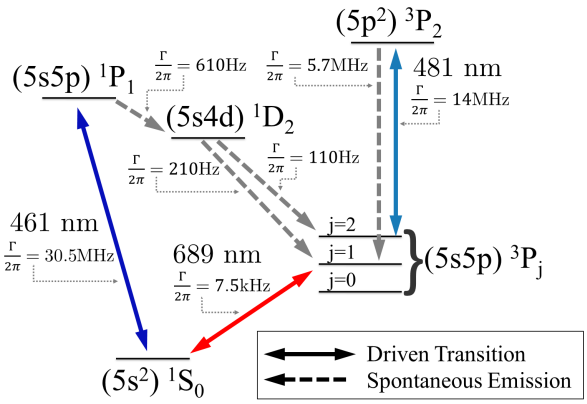

Figure 3.3 : Schematic of PAS light generation

Properties of strontium. Left: Natural abundances and s-wave scattering lengths for all mixtures of Sr. Right: Simplified energy level diagram of Sr showing the relevant states used for trapping and cooling of the atomic gas

and coupled into a single-mode polarization maintaining optical fiber. THis fiber output is luanched near the science chamber and the light output level is continuously monitored via a beam sampler and photodiode placed between the fiber output and the chamber.

Primary reasons why we can't scan large distances. There will be a slight misalignment of the beams into the fiber and the RF may start to fall off. For these experiments an AOM with a center frequecny of 90 MHz was used.

This simple system has many advantages and a couple of drawbacks. Since both photons are aligned into the same fiber then they are gauranteed to have the same output wavevector and therefore the two photon process will be doppler free (since the absorption and emission processes will exactly cancel each other out).

This is a simple system for generating multiple frequencies which are gauranteed to share the same wavevector, phase coherence, and gross frequency stability. Use of the AOM provides highly accurate control of the difference frequency with RF precision.

While versatile and simple, we are worried about the balnace of the RF power onto the AOM. THese devices are narrowband modulators (simple ones)

We see a reduction in contrast when the two drive frequencies differ by more than ≈250 kHz.

Since the modulator is a narrowband device, scann

great care is taken to ensure the maximum amount of contrast is visible on the photodiode. This

As described in some section the slave laser is frequency stabiliezed at +42 MHz of the 86Sr $^1S_0 \rightarrow {}^3P_1$ atomic transition. The AOM then shifts the light the remaining $\approx$ 86 MHz to set the detuning around the $\nu = -2$ bound state of the $^1S_0 + {}^3P_1$ potential. Setting of Δ_1 is done by removing one of the frequencies, peaking up the diffraction angle and alignment into the fiber.

During the course of our experiments we found that mild environmental perturbations (loud noises, air currents due to fans, etc.) to the fiber resulted in slow variation of the light coupling through the fiber. Such amplitude modulations are not uncommon in laser systems and can typically be compensated for by using a closed loop locking mechanism. However, after construction of such a power lock the compoenets did not react quickly enough and there was a significant overshoot

Natural Abundances (%)		Scattering Lengths (a_0)			
		^{84}Sr	^{86}Sr	^{87}Sr	^{88}Sr
0.56	^{84}Sr	122.76	31.65	-57.61	1658
9.86	^{86}Sr	~	798	162.25	97.37
7.00	^{87}Sr	~	~	96.2	54.82
82.58	^{88}Sr	~	~	~	-2

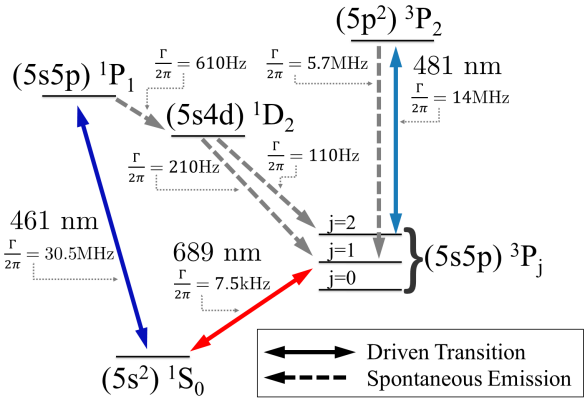

Figure 3.4 : Histogram of PAS beam intensity variation

One of the histograms from onenote. There are separate histograms for each experimental run (I should combine this so I don't have to disucss)

which resulted in an uncontrolled amount of light illuminating the atoms during short exposures. This led us to implement a digital based sample and hold mechanism for reduced intensity variability. This system is described in detail in some section. The sample and hold system in combination with the power lock provided intensity stability with a standard 5% standard deviation during a typical experiment. Fig shows a typical histogram of the recorded intensities.

Make sure to discuss how I scanned the rf frequencies since there is a difference to increasing the freq difference. Since we used the -1 order of the AOM, increasing the frequency of the drive relative to the gross actually lowered the amount of energy in the system, resulting in effectively scanning Δ_1 instead of keeping it fixed. This resulted in a slight variation of the AC stark shift from the intermediate state that can be seen in the strong coupling experiments that are discussed in some section.

Natural Abundances (%)		Scattering Lengths (a_0)			
		^{84}Sr	^{86}Sr	^{87}Sr	^{88}Sr
0.56	^{84}Sr	122.76	31.65	-57.61	1658
9.86	^{86}Sr	~	798	162.25	97.37
7.00	^{87}Sr	~	~	96.2	54.82
82.58	^{88}Sr	~	~	~	-2

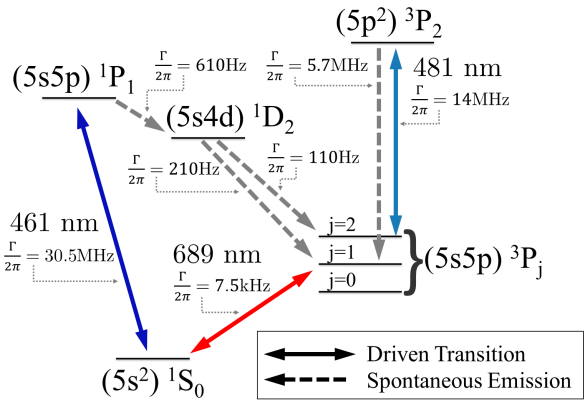

Figure 3.5 : Characteristic view of the PA beatnote

This is the picoscope plot of the beatnote

The beat signal of the two light fields after the fiber is monitored on a photodiode and the rf powers are adjusted to ensure matched intensities for the two frequency components ($I_1 = I_2 \equiv I$).

Chapter 4

Binding energy of the $^{86}Sr_2$ halo molecule

4.1 Probing the ground state potential

Strontium is a nice atom to work with because of the various properties of all of it's isotopes but access to such a variety of properties also comes with it share of complications. The most abundant isotope, 88, has a nearly vanishing scattering length but served as the workhorse for many of our previous stuides and those of other labs. The known scattering properties of strontium are mass scaled from 88 is this somehow not as good for 86? Also, where are the most up to date scattering lengths for Sr from? - The '10 Fourier paper but by probing the 86 ground state potential directly we can obtain a more accurate measurement of the 86-86 scattering length.

Additionally, by utilizing the narrow intercombination potential we are able to detune many linewidths from the intermediate state, thereby

Two-photon photoassociation

umm, I want to write something about the narrow line letting us probe this but

As described in previous chapters, two-photon PAS can be used to directly populate low-lying molecular levels. Applying this technique to strontium 86 we can

explore a similar regime

conclusion of chapter 4 is that we measured the binding energy more accurately which can be directly related to a more precious value of the scattering length for 86. Also there is a straightforward experiment available to use to attempt to measure the efimov paramter for strontium.

how did we determine the binding energy? how did we measure spectra?

Weakly bound ground-state dimers are of great interest in ultracold atomic and molecular physics. In the extreme case of a scattering resonance, the least-bound state represents an example of a quantum halo system [3] with spatial extent well into the classically forbidden region. Halo molecules show universality, meaning that molecular properties such as size and binding energy can be parameterized by a single quantity, the s-wave scattering length a, independent of other details of the atom-pair interaction [4, 5]. For potentials that asymptote to a van-der-Waals form, an additional parameter, the van der Waals length l_{vdW}, can be introduced for a more accurate description. Efimov trimers also exist in systems near a scattering resonance, influencing dimer and atomic scattering properties and introducing additional universal phenomena [6, 7]. Ultracold halo molecules are often associated with magnetic Feshbach resonances [**?**], for which the scattering state and a bound molecular state can be brought near resonance by tuning a magnetic field.

Here we study the least-bound vibrational level of the $X^1\Sigma_g^+$ electronic ground state of the $^{86}Sr_2$ dimer (Fig. 4.1), which is a naturally occurring halo molecule, meaning it exists in the absence of tuning with a magnetic Feshbach resonance. A

well-known example of a naturally occurring halo molecule is the $^4He_2$ dimer [8, 9, 4]. The least-bound vibrational level of the ground state of $^{40}Ca_2$, which was recently studied using similar methods [10], is also very close to this regime.

There are important differences between halo molecules associated with magnetic Feshbach resonances and the naturally occurring halo molecule in ^{86}Sr. With magnetic Feshbach resonances, the relevant scattering and bound molecular states lie on different molecular potentials, and single-photon magnetic-dipole transitions can be used to measure molecular binding energies with RF or microwave spectroscopy [**?** 11**?**]. Typically, this is done by first forming molecules through magneto-association and then driving bound-free or bound-bound transitions converting the halo molecule into a different state. Other methods include spectroscopy with an oscillating magnetic field [**?**], a modulated optically controlled Feshbach resonance [12], and Ramsey-type measurements of atom-molecule oscillation frequencies [13]. It is also possible to efficiently populate halo states with a magnetic-field sweep [14] or evaporative cooling [15] near a magnetic Feshbach resonance [**?**]. These are powerful techniques for manipulating quantum gases of alkali metals and other open-shell atoms, for which there are many magnetic Feshbach resonances. Strontium, however, due to its closed-shell electronic structure, lacks magnetic Feshbach resonances in the electronic ground state.

In this work, we probe the halo state in ^{86}Sr using two-photon Raman photoassociation (PA) [**?**], in which two laser fields couple colliding atoms to the least-bound state of the ground molecular potential. We tune near resonance with an intermediate state that is bound in the 0_u potential corresponding to the $^1S_0 + {}^3P_1$ asymptote

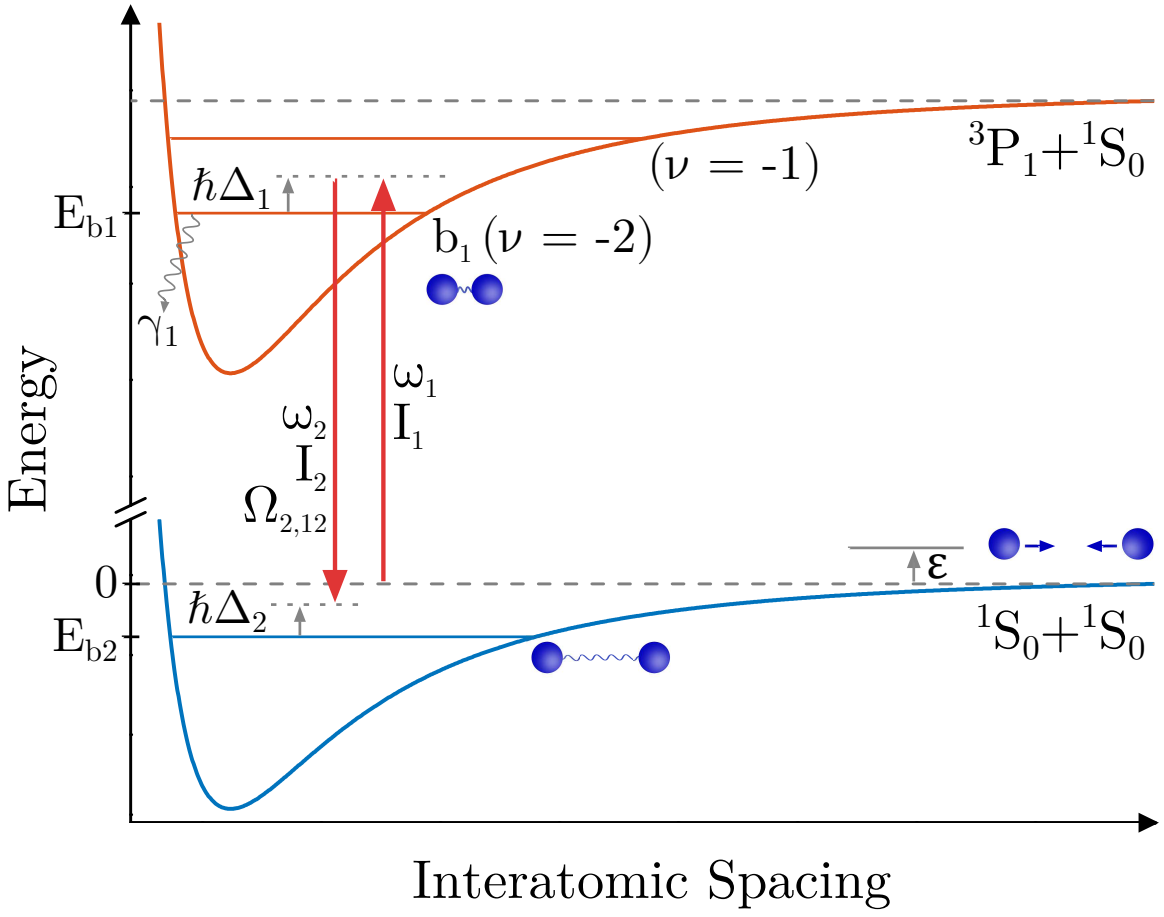

Figure 4.1 : Strontium PAS potential

Two-photon photoassociation diagram . The energy of two well-separated $^1S_0$ atoms at rest is taken as zero. ϵ is the kinetic energy of the colliding atom pair. E_{b1} is the unperturbed energy of the bound state of the excited molecular potential that is near resonance with the free-bound laser, which in these experiments is the second-least bound level of the excited molecular potential ($\nu = -2$). E_{b2} (< 0) is the unperturbed energy of the least bound state of the ground molecular potential. The photon of energy $\hbar\omega_1$ is detuned from E_{b1} by $\hbar\Delta_1$ for $\epsilon = 0$, while the two-photon detuning from E_{b2} is $\hbar\Delta_2$. The decay rate of b_1 is γ_1. Stark and collisional frequency shifts are neglected in this schematic.

at long range [**?**] (Fig. 4.1). We accurately determine the $^{86}Sr_2$ binding energy, considering possible collisional frequency shifts and AC Stark shifts due to trapping and excitation lasers. Using the universal prediction for the binding energy, including corrections derived for a van der Waals potential [16, 17, 18], we derive a more accurate value of the s-wave scattering length for ^{86}Sr atomic collisions [19**?**].

4.2 Experimental setup

Regarding the general process

Using the $^1S_0 + {}^3P_1$ interatomic potential, we perform a raman process using the $\nu = -2$ bound state which has a binding energy of $E_b = -44$MHz cite improved binding en. Sample pre

We used strontium 86 in a thermal gas at temperatures between 30 and 1000 nK. Typical peak densitieis were around $n_0 = 1 \times 10^{12}\,\mathrm{cm}^{-3}$.

Raman process using the second bound state of the $^1S_0 + {}^3P_1$ interatomic potential

What atom do we use what is the sample conditions what trap do we use what are the dimensions of the trap what are the trap freq how do we determine

Two-photon spectroscopy is performed on ultracold ^{86}Sr atoms in a single-beam optical dipole trap (ODT) generated from a 1064-nm laser propagating perpendicular to gravity with beam waists of 260 μm and 26 μm [**? ?**]. The tight waist provides vertical confinement. The trap depth after an evaporative cooling stage determines the sample temperature, which is set between $30 - 1000$ nK. Typical atom

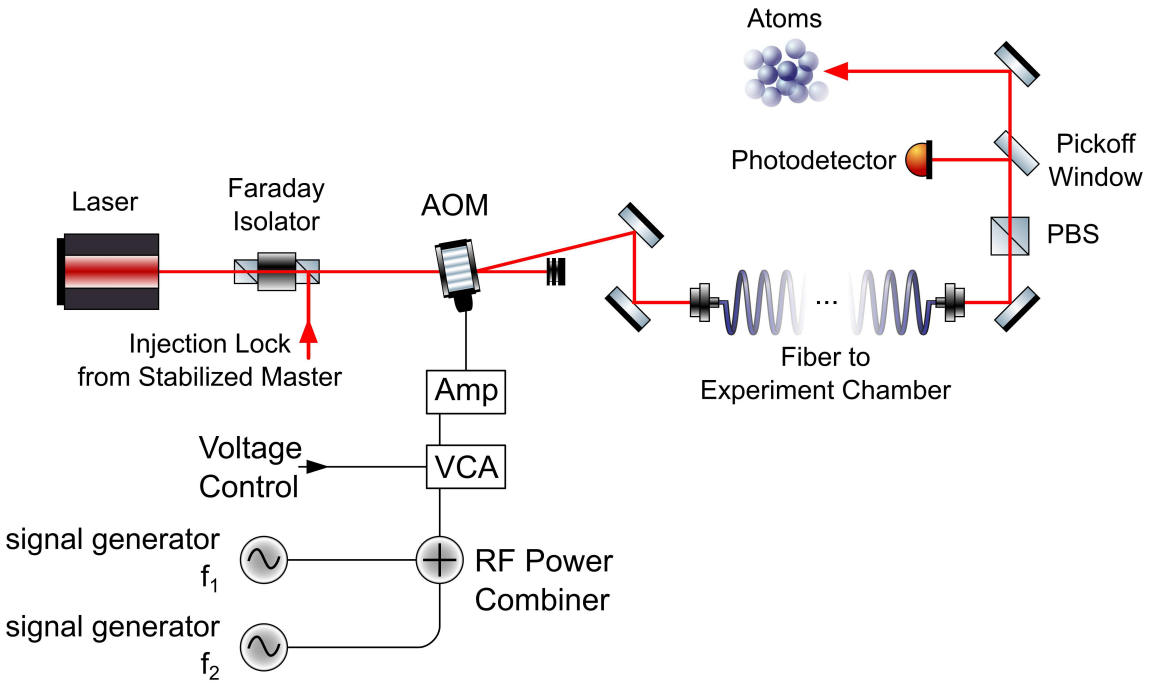

Figure 4.2 : PAS laser setup

Photoassociation laser schematic . A master laser is frequency-stabilized via saturated absorption spectroscopy to the $^1S_0$-$^3P_1$ atomic transition. After amplification with a diode slave laser, light at two controllable frequencies is generated with a single acousto-optic modulator (AOM) and delivered to the atoms with an optical fiber. The beat note between the two frequencies is monitored after the fiber.

numbers are several hundred thousand and peak densities are as high as 2×10^{12} cm^{-3}. The number of atoms and sample temperature are measured using time-of-flight absorption imaging operating on the $^1S_0$-$^1P_1$ transition. Trap oscillation frequencies are determined by measuring dipole and breathing collective mode frequencies, which allow determination of trap volume and sample density.

4.2.1 Photoassociation

After the atoms have equilibrated in the final ODT configuration, the PA lasers are applied (Fig. 4.1). A single acousto-optic modulator, driven with two RF frequencies, is used to generate both PA beams. Light is derived from a frequency-stablized master laser (Fig. 4.2) and coupled into a single-mode optical fiber with output optics that yield a $320\,\mu$m waist at the atoms, much larger than the size of the atom cloud. Both PA beams are linearly polarized along the same direction. The beat signal of the two light fields after the fiber is monitored on a photodiode and the RF powers are adjusted to ensure matched intensities for the two frequency components ($I_1 = I_2 \equiv I$).

The sample temperature is low enough that collisions are entirely s-wave. The target state for the two-photon transition has total angular momentum $J = 0$ and binding energy $E_{b2}(< 0)$. ^{86}Sr has no nuclear spin and a $^1S_0$ electronic ground state, leading to a single ground electronic molecular potential ($\mathrm{X}^1\Sigma_g^+$). The dominant intermediate state (b_1) is the $J = 1$ rotational state of the second least-bound ($\nu = -2$) vibrational level on the 0_u^+ molecular potential, which asymptotically connects to the $^1S_0$-$^3P_1$ atomic transition at long range. This state is bound by $44.246(10)\,$MHz [**?**]. We define $\Delta_1 = \omega_1 - E_{b1}/\hbar$ and $\Delta_2 = \omega_1 - \omega_2 - E_{b2}/\hbar$ as the one-photon detuning from state b_1 and two-photon detuning from state b_2 respectively for an initial scattering state with collision energy $\epsilon = 0$. $\Omega_{2,12}$ is the Rabi frequency for coupling between states b_1 and b_2 due to the laser field at ω_2 with single-beam intensity I_2. Because the binding energy of the halo molecule is very small compared to Δ_1, both laser frequencies are near resonance with the $\nu = -2$ state. The transitions to the least-bound ($\nu = -1$) $J = 1$ excited molecular state, bound by $1.633(1)\,$MHz, and the

excited atomic state lie near enough in energy that they can effect our observations.

Photoassociation leads to loss of atoms from the trap through radiative decay from the intermediate, excited electronic state, and from collisions between molecules and background atoms. The PA spectrum is obtained by holding ω_2 fixed and varying ω_1, which varies Δ_2 across resonance (Fig. 4.1). Δ_1 thus also varies slightly during a scan, but the spectra are so narrow compared to Δ_1 that we neglect this in our analysis. After an exposure time on the order of one hundred milliseconds, the number of ground-state atoms remaining and the sample temperature are measured with time-of-flight absorption imaging.

4.2.2 Consideration of the trap depth

Show plots of the trap and how we determined what the trap depth was

Our previous discussion of the rate loss constant assumed we could describe the spatial distribution of the atomic density profile analytically. This is a valid supposition given two key assumptions, 1) the sample termperature remains constant during the PA exposure and 2) the trap is of sufficient depth that we can reasonably approximate it as a harmonic trap. cite Mi's trap paper.

Analysis of the trapping conditions after acquisition of the data revealed that this second assumption was not maintained during our experiment. In some figure we can see that we only have an eta of 2. This is troublesome as it means we must numerically consider the density distribution over space when solvinf for the rate loss constant K.

In addition to the modified spatial distribution, we must also consider the

effect of the trap depth on the energy profile of the trapped gas. In a typical high-eta trap, a typical Boltzmann profile is sufficient to describe the velocity distribution of the atoms and when we consider the distribution of relative energies that is important for PAS expeirments, we recover a simple bolztmann weighting for the distribution of energy probabilities. This is shown in sopme app.

However, the case of a low-eta trap we must define a local cutoff energy at each point in space within the trap as atoms that have an energy higher than the local eta value are assumed to be lost from the trap. Derivation of this truncated relative energy probabillity distribution is given in some app and results in a stronger weighting of the coldest atoms near the bottom of the trap.

4.3 Theoretical description

This section develops the more groddy form of the BJ equation. Include the

In Ch. somewhere we discussed the usual situation for observing loss due to photoassocition. This experiment was similar to the 88 autler townes experiment.

PA loss is described with a local equation for the evolution of the atomic density

$$\dot{n} = -2Kn^2 - \Gamma n, \tag{4.1}$$

where the laser-frequency dependence of the collision-event rate constant, K, determines the spectrum of the PA loss. The one-body loss rate, Γ, is due to background collisions and off-resonant scattering from the PA lasers. By integrating this equation over the trap volume, we can obtain the evolution of the total number of trapped

atoms

$$N(t) = \frac{N_0 \mathrm{e}^{-\Gamma \mathrm{t}}}{1 + \frac{2\mathrm{N}_0 \langle \mathrm{K} \rangle \mathrm{V}_2}{\Gamma \mathrm{V}_1^2}(1 - \mathrm{e}^{-\Gamma \mathrm{t}})} \tag{4.2}$$

where N_0 is the number of trapped atoms at the beginning of the PAS interaction time. The effective trap volumes V_q are

$$V_{\mathrm{q}} = \int_{\mathrm{V}} d^3 r \, e^{-\frac{qU(\mathbf{r})}{k_B T}}, \tag{4.3}$$

for trapping potential $U(\mathbf{r})$. $\langle K \rangle$ is the trap-averaged collision event rate constant

$$\begin{aligned} \langle K \rangle &= \frac{1}{V_2} \int_{\mathrm{V}} d^3 r \, e^{-\frac{2U(\mathbf{r})}{k_B T}} \\ &\quad \times \frac{1}{h \, Q_T} \int_0^{\epsilon_{\max}(\mathbf{r})} d\epsilon |S|^2 \, e^{-\epsilon / k_B T}, \end{aligned} \tag{4.4}$$

which is itself a thermal average of the scattering probability for loss ($|S(\epsilon, \omega_1, \omega_2, ..., \mathbf{r})|^2$) over the collision energy ϵ, with an energy cutoff $\epsilon_{\max}$ to be discussed momentarily. The trapping potential is given by $U(\mathbf{r}) = mgz + h\chi_{1064,\mathrm{g}} I_{1064}(\mathbf{r}) - \tilde{U}_{\min}$, where mgz is the gravitational potential at height z, $I_{1064}(\mathbf{r})$ is the intensity of the trapping light, and $\chi_{1064,\mathrm{g}} = 11\,\mathrm{Hz}/(\mathrm{W/cm}^2)$ [**?**] is proportional to the polarizability of ground state atoms due to 1064 nm light. $\tilde{U}_{\min}$ is subtracted to set the potential at the trap minimum to zero. The spatial integral is restricted to regions around the trapping local minimum with $U(\mathbf{r})$ less than the trap depth [**?**]. Downhill regions on the other side of the saddle point defining the trap depth are excluded. The laser intensity profile is measured independently, and the potential is found to be consistent with measured trap oscillation frequencies. The partition function is $Q_T = \left(\frac{2\pi k_B T \mu}{h^2}\right)^{3/2}$ for reduced mass $\mu = m/2$ and sample temperature T, for atoms of mass m.

Equation (4.4) provides the correct thermal average when the collision-energy distribution does not need to be truncated ($\epsilon_{\max} \to \infty$). For our data, however, the

ratio of sample temperature to trap depth is $k_B T/U_{\rm depth} \approx 3$ for samples with temperature above 100 nK and drops to unity for 30 nK samples, so truncation effects are important. If the single-particle kinetic-energy distribution function is a Boltzmann truncated at $U_{\rm depth} - U(\mathbf{r})$, then the collision-energy distribution follows a Boltzmann distribution at low energies [$\epsilon \ll U_{\rm depth} - U(\mathbf{r})$] and falls off more quickly at larger energies, reaching zero at $2[U_{\rm depth} - U(\mathbf{r})]$. We find that this treatment predicts a narrower distribution on the red side of the spectral line than we observe in our data, suggesting the presence of atoms in non-ergodic orbits with energies above the saddle point of the trap. This is not surprising given the large collisional loss rate associated with near-resonant scattering in this isotope. Fortunately, the molecular binding energy is strongly determined by the sharp edge of the spectrum on the blue side of the line, which is relatively insensitive to the description of the red tail. Our data is fit well with a truncated Boltzmann distribution of collision energies [Eq. (4.4)]. To estimate the systematic uncertainty introduced by this treatment, we perform fits with $\epsilon_{\rm max}$ equal to $2[U_{\rm depth} - U(\mathbf{r})]$ and $U_{\rm depth} - U(\mathbf{r})$ and take the mean of the two results as the best value for the binding energy and half the difference as a systematic uncertainty $\sigma_{\epsilon_{\rm max}} \approx 100\,{\rm Hz}$. This procedure does not correctly represent the overall normalization of $\langle K \rangle$, but we are not concerned with overall signal amplitude in this study. Atom temperatures vary by no more than 20% during the interaction time, so assuming a constant sample temperature is reasonable.

Bohn and Julienne [**?**] provide an expression for $|S(\epsilon, \omega_1, \omega_2, ...)|^2$ for a collision on the open channel of two ground state atoms (g) with total energy ϵ leading to loss-

producing decay from the excited state b_1 with rate γ_1 (Fig. 4.1),

$$|S|^2 = \frac{(\Delta_2 + \epsilon/\hbar)^2 \gamma_1 \gamma_s}{\left[(\Delta_1 + \epsilon/\hbar)(\Delta_2 + \epsilon/\hbar) - \frac{\Omega_{12}^2}{4}\right]^2 + \left[\frac{\gamma_1+\gamma_s}{2}\right]^2 (\Delta_2 + \epsilon/\hbar)^2}. \tag{4.5}$$

For simplicity, we have omitted the light shift of b_1 due to coupling to the scattering continuum [**?**]. This approach was found to be sufficient for describing two-photon spectroscopy to a more deeply bound molecular level in ^{88}Sr [**?**]. Equation (4.5) neglects all light shifts due to the trapping laser. Light shifts due to the photoassociation lasers coupling to states outside our model (Fig. 4.1) are also neglected. The thermal energy is much greater than the zero-point energy for trap motion, $T \gg h\nu_{\rm trap}/k_B$, so confinement effects are negligible [**?**]. $\gamma_1 = 2\gamma_{\rm atomic}$, where $\gamma_{\rm atomic} = 4.7 \times 10^4\,{\rm s}^{-1}$ is the decay rate of the atomic $^3P_1$ level. $\gamma_s(\epsilon)$ is the stimulated width of b_1 due to coupling to the initial scattering state by laser 1, which for low energy can be expressed as [20**?** , 10]

$$\gamma_s(\epsilon) = 2k l_{\rm opt} \gamma_1, \tag{4.6}$$

where the optical length ($l_{\rm opt} \propto I_1$) is related to the overlap between the initial colliding state and b_1, and $k = (2\mu\epsilon)^{1/2}/\hbar$. We take the intermediate state b_1 as the $\nu = -2$ state, for which $l_{\rm opt}/I = (1.5 \pm 0.3) \times 10^4\, a_0/({\rm W/cm^2})$ [**?**], where $a_0 = 5.29 \times 10^{-11}\,{\rm m}$ is the Bohr radius.

For the experiments reported here, we maintain significant intermediate-state detuning, Δ_1, for which $|\Delta_1| \gg |\Omega_{2,12}|$. Thus we are in a Raman configuration, and not in the Autler-Townes regime [**?**]. In the Raman regime, Eq. 4.5 shows a maximum near two-photon resonance at $\Delta_2 + \epsilon/\hbar = \Omega_{2,12}^2/4\Delta_1$. Following a treatment discussed

recently for a similar experiment in calcium [10], if the detuning is restricted to near two-photon resonance then $|S|^2$ can be approximated as a Lorentzian

$$|S|^2 \approx \frac{A(\epsilon)}{\left(\Delta_2 + \epsilon/\hbar - \frac{\Omega_{12}^2}{4(\Delta_1+\epsilon/\hbar)}\right)^2 + \left[\Gamma_L(\epsilon)/2\right]^2}, \tag{4.7}$$

where

$$A(\epsilon) = \frac{\Omega_{2,12}^4 \gamma_1 \gamma_s(\epsilon)}{16(\Delta_1 + \epsilon/\hbar)^4} \tag{4.8}$$

$$\Gamma_L(\epsilon) = \frac{\Omega_{2,12}^2[\gamma_1 + \gamma_s(\epsilon)]}{4(\Delta_1 + \epsilon/\hbar)^2}. \tag{4.9}$$

In practice, the variation of collision energy is negligible compared to the one-photon detuning Δ_1.

There are several concerns regarding the rigorous application of the Bohn and Julienne theory [**?**] to our experiment. The obvious one is that it assumes an isolated intermediate state, which is not always a good approximation because of the proximity of state b_1 to the $^1S_0 + {}^3P_1$ asymptote and to the $\nu = -1$ state. Because of the small decay rate γ_1 of the intermediate molecular state associated with metastable $^3P_1$ atomic state, we also expect that loss from the ground molecular state cannot be neglected.

The more subtle issue is that Eq. (4.7) is derived assuming only a single laser beam is near resonant with each leg of the two-photon transition, which is not a good approximation for two-photon spectroscopy of a halo state and the resulting small laser-frequency difference $\omega_1 - \omega_2 \approx -E_{b2} \ll |\Delta_1|$. We can expect that coupling between pairs of states due to both photoassociation lasers will contribute to the transition strength and light shifts of the levels induced by the photassociation lasers [**? ?**].

In the absence of a more complete theory treating these effects, we analyze loss spectra using the effective expression given by Eq. (4.10), where the observed molecular binding energy (E'_{b2}) includes any perturbations due to AC Stark or collisional

$$|S|^2 = \frac{\Gamma_L(\epsilon) + \gamma_{\text{eff}}}{\Gamma_L(\epsilon)} \times \frac{\eta A(\epsilon)}{(\omega_1 - \omega_2 + \epsilon/\hbar - E'_{b2}/\hbar)^2 + \left[\frac{\Gamma_L(\epsilon)+\gamma_{\text{eff}}}{2}\right]^2}, \tag{4.10}$$

shifts.

Parameters have been added in Eq. (4.10) to account for deviations of the signal strength (η) and width (γ_{eff}) from the predictions of [**?**]. If deviations from Eq. (4.7) are small, we expect $\eta \sim 1$, $\gamma_{\text{eff}} \sim 0$, and $E'_{b2} \sim E_{b2} + \Omega_{2,12}^2/4(\Delta_1 + \epsilon/\hbar)$.

Light shifts (AC Stark shifts) due to the trapping lasers and collisions with ground-state atoms (density n) should contribute to shifts of molecular resonance. Similar effects were taken into account in a recent, high-precision study of weakly bound molecular states of ultracold ytterbium atoms [21]. In addition, we expect that both 689-nm excitation lasers will shift the line, not just $I_2 \propto \Omega_{2,12}^2$. We model the relationship between the measured resonance positions and the unperturbed binding energy E_{b2} as

$$E'_{b2} = E_{b2} + h\chi_{689} I_{689} + h\chi_{1064} I_{1064}(\mathbf{r}) + h\chi_n n(\mathbf{r}). \tag{4.11}$$

The susceptibilities, in Hz per unit intensity or density, will be determined from experimental data or theoretical considerations. The variation with position of the trapping laser intensity (I_{1064}) and the density give rise to the spatial dependence of $|S|^2$ and the need for a spatial average in Eq. (4.4). We take I_{689} as twice the single-

beam intensity $I_{689} = 2I$. The 689-nm excitation beam is large enough compared to the atom sample to neglect spatial variation. The functional form for the AC Stark shift due to the excitation lasers is discussed in Sec. **??**.

4.4 Spectral fitting and determination of the binding energy

Figure 4.3 shows a series of spectra for different final trap depths and sample temperatures. The characteristic asymmetric lineshape for excitation of a thermal sample is evident, with width decreasing as sample temperature decreases. The molecular binding energy is close to the sharp edge on the blue side of each spectrum.

We fit atom-loss spectra with Eq. (4.2) for the evolution of atom number with time, using the phenomenological expression Eq. (4.10) for the scattering probability and Eq. (4.4) for the average of the collision event rate constant over the trap volume and collision energy. The sample temperature, perturbed resonance frequency E'_{b2}, η, and γ_{eff} are taken as fit parameters. In the final analysis, temperatures are set to values determined from time-of-flight imaging of the atoms, but when they are allowed to vary, the fit values differ by no more than 10%. Approximately 10 spectra are recorded for each set of experimental parameters, and the spread of resulting fit values are used to determine best values and uncertainties.

4.4.1 AC Stark Shift due to Excitation Lasers

The most significant perturbation to the resonance position is the AC Stark shift due to the excitation laser intensity, as shown in Fig. 4.4.1. For this data, the trap parameters, temperature ($T = 30\,\text{nK}$), and initial peak sample density ($n_0 = 2 \times$

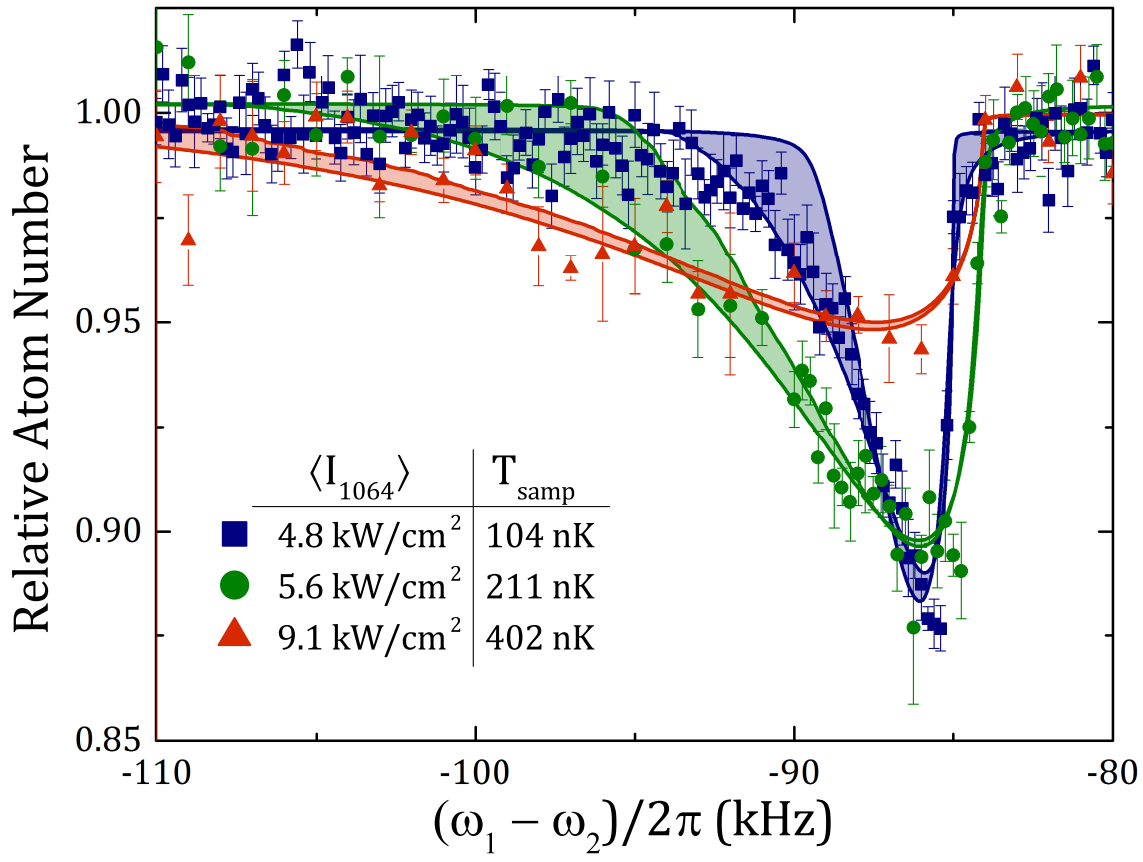

Figure 4.3 : Variation of 1064 nm trap depth

Atom-loss spectra as a function of two-photon difference frequency $(\omega_1 - \omega_2)/2\pi$ for intermediate detuning $\Delta_1/2\pi = -9\,\mathrm{MHz}$. Sample temperature and average trapping laser intensity are indicated in the legend. The single-beam excitation laser intensity is $I = 25\,\mathrm{mW/cm^2}$ for the 104 nK spectrum and $I = 48\,\mathrm{mW/cm^2}$ for the 211 nK and 402 nK spectra. Fits are described in the text, with the two boundaries of each band given by the fits with collision-energy truncation ϵ_{max} equal to $2[U_{\mathrm{depth}} - U(\mathbf{r})]$ and $U_{\mathrm{depth}} - U(\mathbf{r})$.

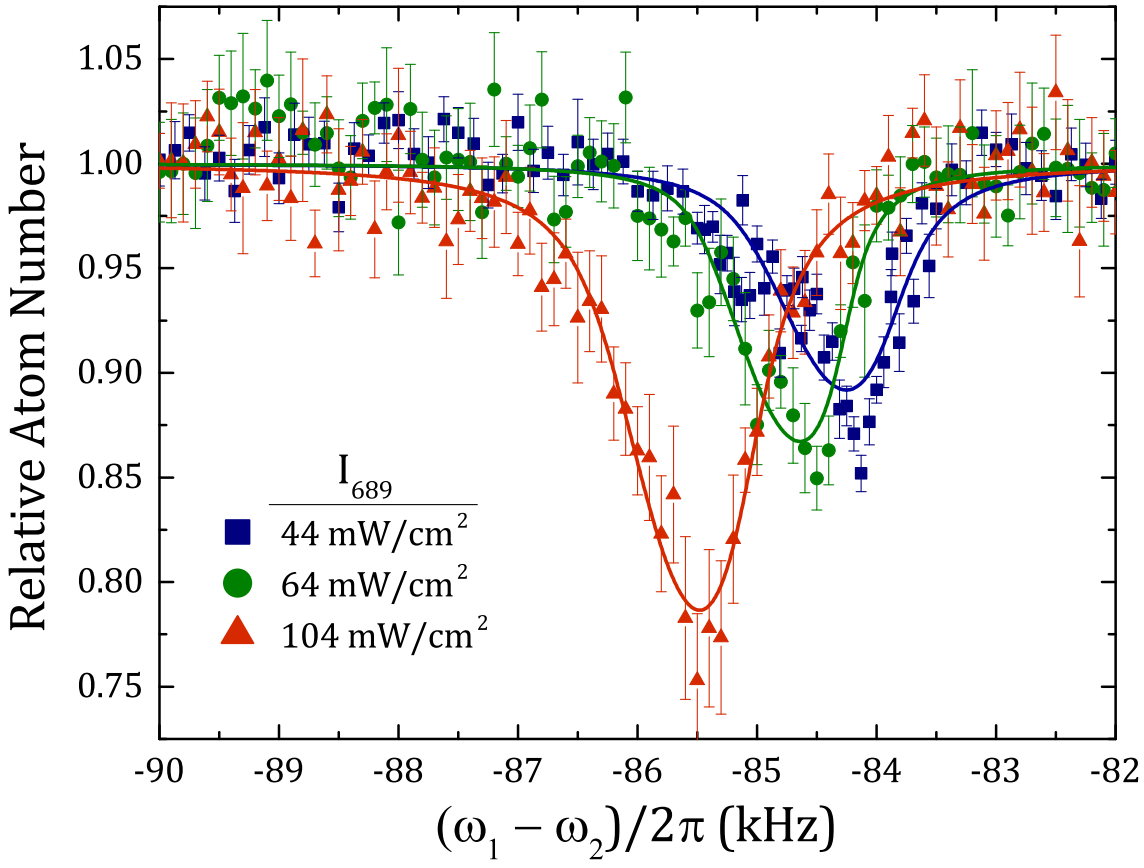

Figure 4.4 : Variation of 689 nm excitation

Atom-loss spectra as a function of two-photon difference frequency $(\omega_1 - \omega_2)/2\pi$ for intermediate detuning $\Delta_1/2\pi = -9\,\mathrm{MHz}$ and various 689-nm excitation laser intensities . Twice the single-beam intensity $I_{689} = 2I$ is indicated in the legend.

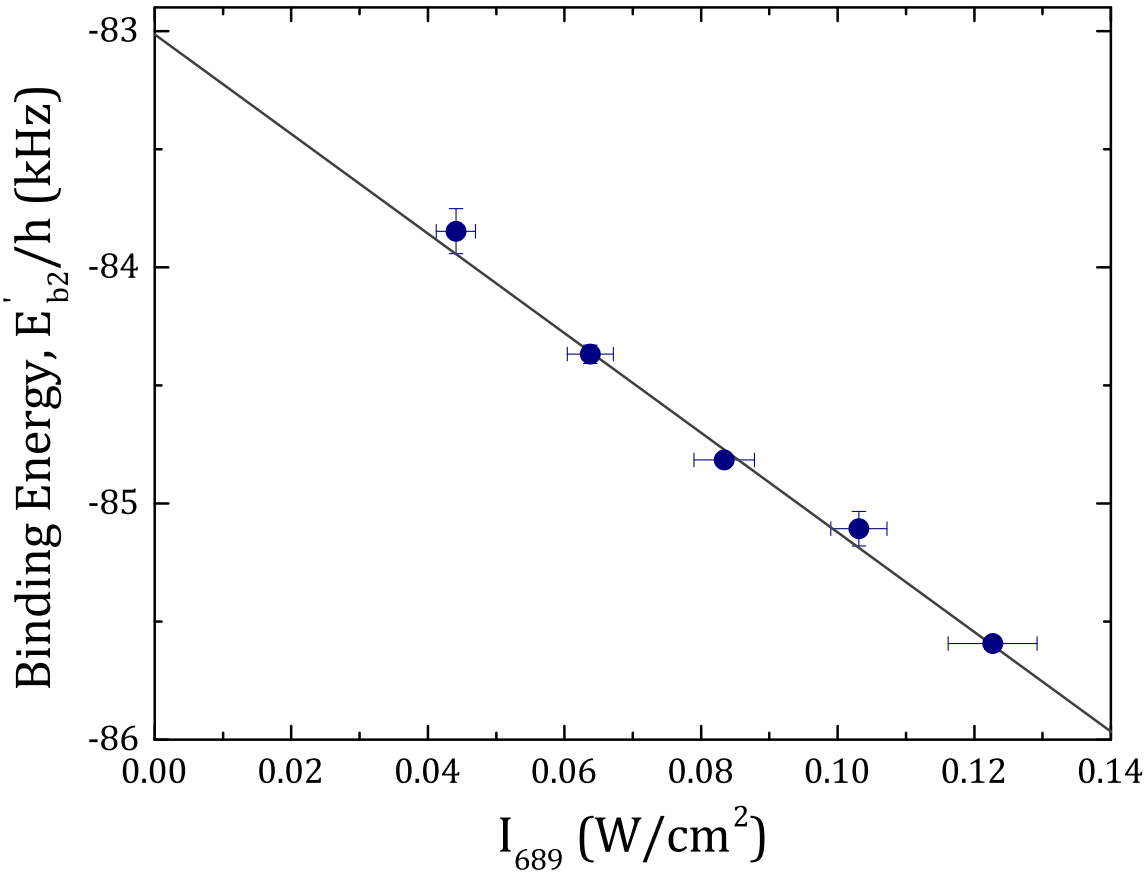

Figure 4.5 : Fit of 689 nm AC Stark shift

Measured resonance position E'_{b2} plotted versus twice the single-beam intensity $I_{689} = 2I$. The linear fit provides the AC Stark shift parameter χ_{689}.

$10^{12}\,\mathrm{cm}^{-3}$) are held constant. We vary the single-beam excitation intensity from $I = 0.02 - 0.06\,\mathrm{mW/cm}^{-2}$, and the excitation time is 50 ms. The observed shifts are comparable to the thermal width of the spectrum, allowing a precise determination of $\chi_{689} = -21(1)(2)\,\mathrm{kHz/(W/cm^2)}$ from a linear fit to the resonance positions, $E'_{b2} \propto h\chi_{689} I_{689}$ (Fig. 4.5). The first quoted uncertainty is statistical and it arises from variations in parameters and fluctuations in the measured intensity during the scans. The second value is systematic, reflecting uncertainty in laser-beam size and intensity profile at the atoms. All parameters beside the 689-nm laser intensity are held fixed for this data set, and the AC Stark shift is not correlated with any other variable, such as density or trap intensity. We thus obtain an accurate measure of χ_{689} without attempting to account for other systematic shifts of E'_{b2} in this data. A study of the dependence of χ_{689} on detuning from the excited molecular state will be discussed in Sec. **??**.

Broadening to the red of the spectrum reflects the distribution of atom-atom collision energies, while broadening to the blue is most sensitive to decay of the intermediate state (Γ_L) and the phenomenological broadening term γ_{eff} [Eqs. (4.9) and (4.10)]. The long lifetime of the excited state and the significant detuning Δ_1 result in a width $\Gamma_L(\epsilon)$ less than 5 Hz for all conditions. This is extremely small compared to observed width, which yields values of γ_{eff} on the order of 300 Hz. We hypothesize that this width reflects decay of molecules in the electronic ground-state due to collisions with background atoms.

4.4.2 Density-dependent Frequency Shift

A shift of the two-photon resonance position is possible due to differing mean-field shifts of initial atomic and final molecular states arising from interaction with the background of ground-state atoms. Such a shift would be proportional to the atom density and depend upon the s-wave scattering lengths for atom-atom and atom-dimer collisions, a_{86} and $a_{\rm ad}$ respectively. This was observed in a Rb Bose-Einstein condensate (BEC) in [22]. For a non-degenerate gas, this effect yields $\chi_n = \hbar(\frac{a_{\rm ad}}{\mu_{\rm ad}} - 4\frac{a_{86}}{\mu_{\rm aa}}) = \frac{\hbar}{m}(\frac{3}{2}a_{\rm ad} - 8a_{86})$, where $\mu_{\rm ad}$ and $\mu_{\rm aa}$ are the reduced masses for molecule-atom and atom-atom collisions respectively. Note that the shift would vanish for $a_{\rm ad} = (16/3)a_{86}$.

The largest density used in our experiment ($\sim 1 \times 10^{12}\,{\rm cm}^{-3}$) is relatively low compared to typical BEC densities, and at this time we are unable to accurately measure a variation of resonance position with density. However, the atom-atom scattering is close to resonance and thus Efimov physics can provide information on $a_{\rm ad}$ [6, 7] and an estimate of the systematic error introduced by any residual density-dependent frequency shifts. For a zero-range interaction, the atom-dimer scattering length is related to the atom-atom scattering length through the three-body Efimov parameter κ_* according to [6]

$$a_{\rm ad} = a_{86}\left\{1.46 + 2.15{\rm cot}[s_0{\rm ln}(14.1\kappa_* a_{86})]\right\} \tag{4.12}$$

where $s_0 = 1.006$ *.

*The Efimov parameter is related to E^0_{3b} through $\kappa_* = (m|E^0_{3b}|/\hbar^2)^{1/2}$, where E^0_{3b} is the binding energy the lowest Efimov trimer would have in the case of resonant atom-atom interactions.

In principle, the atom-dimer scattering length can take any value. However, for a deep atom-atom potential, such as for the ground-state strontium dimer [19], there is a universality of the three-body physics that sets $\kappa_* = 0.226(2)/l_{\mathrm{vdW}}$ [23]. Here, $l_{\mathrm{vdW}} = (2\mu C_6/\hbar^2)^{1/4}/2 = 74.6\,a_0$ is the van der Waals length associated with the C_6 coefficient of the long-range Sr_2 ground-state potential. We use $C_6 = 3.03(1) \times 10^{-76}$ $\mathrm{J\,m^6}$ found from a fit of potential parameters to spectroscopic data [19], which is consistent with a recent *ab initio* calculation [24]. This yields $\kappa_* = 5.72 \times 10^7\,\mathrm{m^{-1}} = (330\,a_0)^{-1}$. Equation (4.12) then predicts $a_{\mathrm{ad}} = 6.4\,a_{86}$, which leads to a small density-dependent frequency shift parameter of $\chi_n = 50\,\mathrm{Hz}/(10^{12}\,\mathrm{cm^{-3}})$. A numerical calculation including a finite-range correction for the atom-atom interaction [25] results in $a_{\mathrm{ad}} = 3.5\,a_{86}$ and $\chi_n = -90\,\mathrm{Hz}/(10^{12}\,\mathrm{cm^{-3}})$. Thus, a very small shift is expected for the densities used here. We incorporate $\chi_n = 0 \pm 90\,\mathrm{Hz}/(10^{12}\,\mathrm{cm^{-3}})$ as a set parameter in our model of the spectrum, where we set the systematic uncertainty to reflect the spread of theory predictions. This uncertainty will be significant for our determination of the unperturbed halo binding energy.

4.4.3 Unperturbed Halo Binding Energy and AC Stark Shift due to Trapping Lasers

With an accurate determination of χ_{689} and a value for χ_n, we use the data shown in Fig. 4.3 to determine the susceptibility for the AC Stark shift from the trapping laser, χ_{1064}, and the unperturbed halo binding energy E_{b2}. Figure 4.4.3 shows a plot of $E'_{b2} - \chi_{689} I_{689} - \chi_{\mathrm{n}} \langle n \rangle$ versus $\langle I_{1064} \rangle$, where E'_{b2} is the resonance position from each fit and $\langle ... \rangle$ indicates a weighted average of the quantity over the trapped sample, with a weighting given by the square of atom density. This weighting reflects the

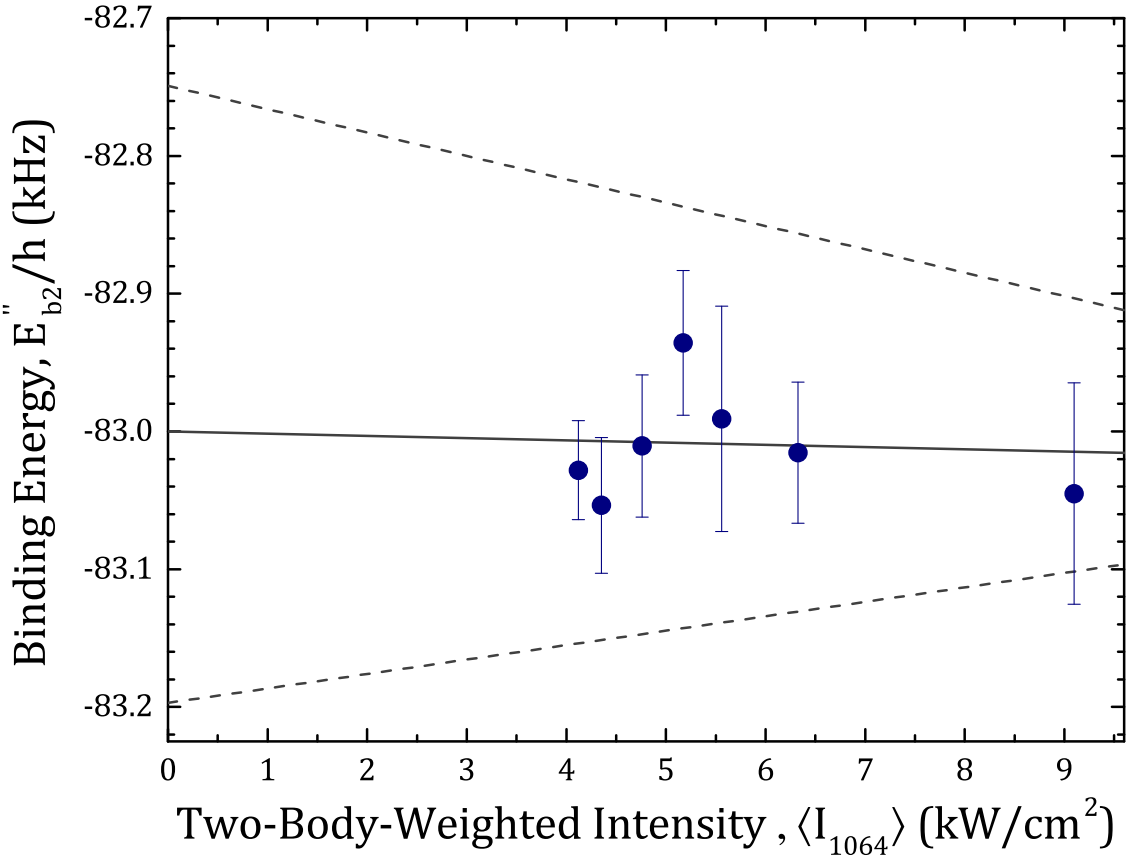

Figure 4.6 : Measurement of halo state susceptibility, χ_{1064}

Measured resonance positions corrected for excitation-laser AC Stark shift and collisional frequency shift, $E'_{b2} - \chi_{689} I_{689} - \chi_n \langle n \rangle$, as a function of average trap laser intensity $\langle I_{1064} \rangle$ for the data such as in Fig. 4.3 . The trend line and confidence intervals are described in the text.

contribution to photoassociative loss, a two-body process. The plotted uncertainties in $E'_{b2} - \chi_{689} I_{689} - \chi_{\rm n} \langle n \rangle$ are from statistical variation in the fit parameters. The typical average density is $\langle n \rangle \approx 1 \times 10^{12}\,{\rm cm}^{-3}$. The linear fit function is to $E_{b2} + \chi_{1064} \langle I_{1064} \rangle$. In addition to statistical uncertainty, we have systematic uncertainty from $\chi_{\rm n}$ and treatment of the truncation of the collision-energy integral [Eq. (4.4)]. The dashed lines shown in Fig. 4.4.3 are resulting fits when the values of $E'_{b2} - \chi_{689} I_{689} - \chi_{\rm n} \langle n \rangle$ are shifted by the sum of these systematic uncertainties. The resulting value for the unperturbed binding energy is $E_{b2}/h = -83.00(7)(20)\,{\rm kHz}$, where the first uncertainty is statistical, and the second is systematic. We observe a susceptibility to I_{1064} of $\chi_{1064} = 0 \pm 10\,{\rm Hz}/({\rm kW/cm^2})$.

4.5 Discussion of binding energy

In the limit of extremely small binding energy, and thus resonant atom-atom interactions, the binding energy of a halo molecule is approximately given by [4]

$$E_b = -\hbar^2 / 2\mu a^2. \tag{4.13}$$

For interactions described at long-range by the van-der-Waals form, $V(r) = -C_6/r^6$, as with ultracold atoms, a convenient figure of merit for quantifying how accurate this simple expression should be is given by the ratio of the s-wave scattering length to the mean scattering length or interaction range, closely related to the van der Waals length through [16, 11]

$$\bar{a} = l_{\rm vdW} \frac{\Gamma\left(\frac{3}{4}\right)}{\sqrt{2}\Gamma\left(\frac{5}{4}\right)}. \tag{4.14}$$

Slightly away from resonance, corrections to the binding energy for the van

der Waals potential were worked out in [17, 18], yielding

$$E_{b2} = -\frac{\hbar^2}{2\mu(a-\bar{a})^2}\left[1 + \frac{g_1\bar{a}}{a-\bar{a}} + \frac{g_2\bar{a}^2}{(a-\bar{a})^2} + ...\right], \tag{4.15}$$

where $g_1 = \Gamma(1/4)^4/6\pi^2 - 2 = 0.918...$ and $g_2 = (5/4)g_1^2 - 2 = -0.947....$ The range of validity of this expression is $a \gtrsim 2\bar{a}$. The accuracy of the first term in this expansion has been experimentally confirmed for various systems such as ^{85}Rb [13, 26], ^{40}K [27, 28] and ^{6}Li [29]. This derivation of Eq. (4.15) assumes that the influence of short-range physics, which can be expressed through a quantum defect, varies negligibly from threshold to the molecular binding energy. We expect this to be an excellent approximation, since, as shown in Ref. [17] the corrections are typically less than about 1% even for GHz binding energies.

For ground-state ^{86}Sr atoms, $\bar{a} = 71.3\,a_0$. The most accurate value available for the s-wave scattering length is $a = 798(12)\,a_0$ [19], satisfying the requirement of $a \gg \bar{a}$ for the least-bound state on the ground molecular potential to be a halo molecule. Nonetheless, $\bar{a}/(a-\bar{a}) = .10$, and the corrections given by Eq. (4.15) are significant. Figure 4.5 shows the importance of the correction terms.

Equation (4.15) and the previous best value of the scattering length [19] predict a binding energy of $E_{b2} = -86(3)\,\mathrm{kHz}$. This agrees with our measurement, but by inverting Eq. (4.15), we can use our increased accuracy in E_{b2} to extract an improved value of the scattering length of $a = 810.6(3)(9)\,a_0$, where uncertainties reflect statistical and systematic uncertainties in E_{b2} respectively. The next higher-order term in $x_0 = \bar{a}/(a-\bar{a})$ is likely to introduce a correction on the order of 100 Hz in Eq. (4.15), creating a systematic uncertainty in a that is about one third of the uncertainty from our measurement.

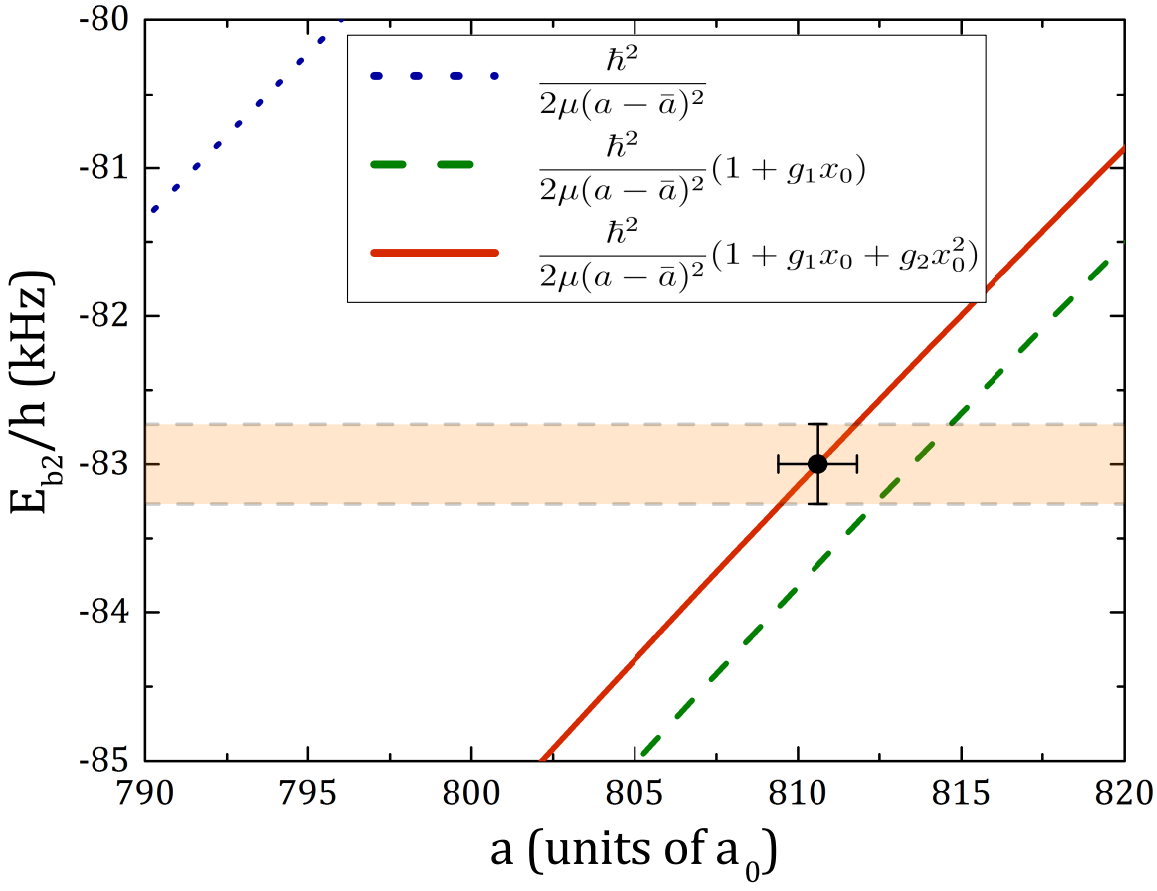

Figure 4.7 : Determination of 86 scattering length

Halo binding energy versus s-wave atom-atom scattering length for ^{86}Sr . The shaded region indicates our experimental measurement. The lines are predictions of Eq. 4.15 retaining up to the first, second, and third terms as indicated in the legend $[x_0 = \bar{a}/(a-\bar{a})]$. The data point is the prediction of Eq. (4.15) for the recommended value of the measured binding energy.

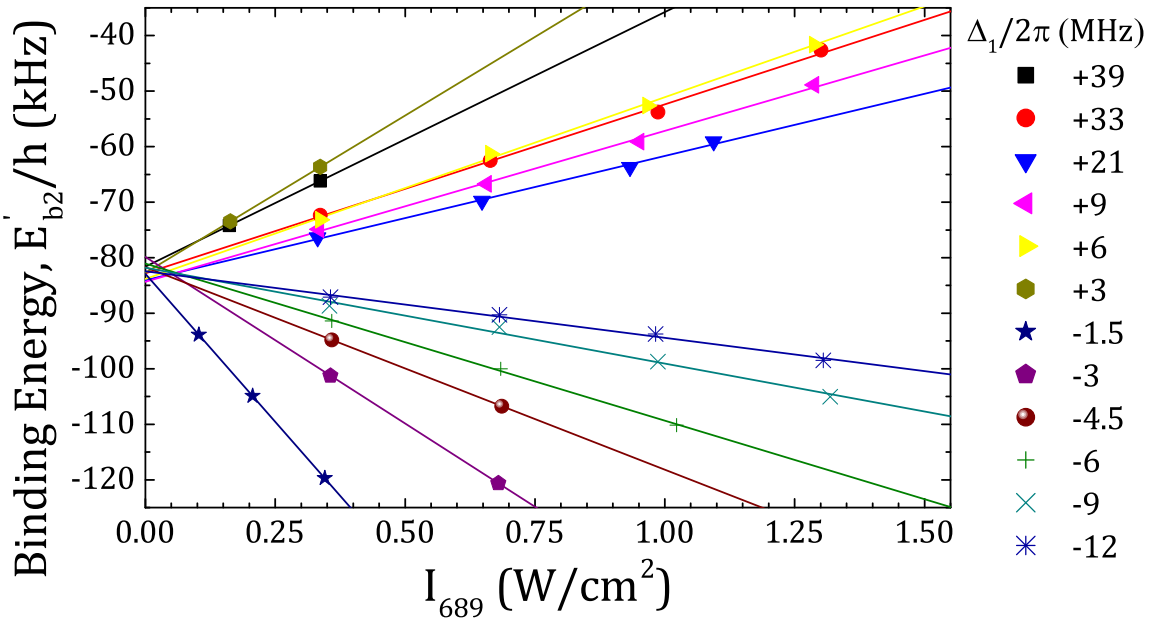

Figure 4.8 : Variation of halo susceptibility as a function of Δ_1

Two-photon PA resonance positions as a function of twice the single-beam excitation intensity, $2I = I_{689}$ for various intermediate state detunings, Δ_1 .

4.6 Calculating the bound-bound Frank-Condon factor

The proximity of ^{86}Sr to a scattering resonance and the susceptibility of the halo binding energy to the intensity of the excitation light suggests using light to tune the binding energy and scattering length as was done with optically assisted magnetic Feshbach resonances [30, 12], which is closely related to the use of optical Feshbach resonances [**?** 31, 32, 33, 34]. Understanding the frequency-dependence of χ_{689} is important for investigating this possibility, so we extracted this parameter from spectra at a wide range of 689-nm laser intensities and detuning from the intermediate resonance (Δ_1).

Figure 4.5 shows the resulting resonance positions, E'_{b2}, versus twice the single-beam intensity, $2I = I_{689}$. The shift in molecular binding energy is linear with intensity over the explored range, but varies greatly in magnitude and sign. From linear fits, we extract the AC Stark shift parameter $\chi_{689}(\Delta_1)$ through $E'_{b2} \equiv E_{b2} + h\chi_{689}(\Delta_1)I_{689}$ (Fig. 4.6).

In the experiment, the total 689-nm intensity oscillates with 100% contrast according to $I_{\text{total}} = I_1 + I_2 + 2\sqrt{I_1 I_2}\cos\left[(\omega_1 - \omega_2)t\right] = 2I\left\{1 + \cos\left[(\omega_1 - \omega_2)t\right]\right\}$. The functional form we use to fit the AC Stark shift reflects the time average of the intensity and neglects the interference term. To confirm that this is the correct description, we numerically solved the time-evolution for a three-level system with similar optical couplings and oscillating optical intensity as present during two-photon

PA of a halo state. The Hamiltonian is

$$H = \begin{pmatrix} 0 & \Omega_{01}\left[\cos(\omega_1 t) + \cos(\omega_2 t)\right] & 0 \\ \Omega_{01}\left[\cos(\omega_1 t) + \cos(\omega_2 t)\right] & E_{b1} & \Omega_{12}\left[\cos(\omega_1 t) + \cos(\omega_2 t)\right] \\ 0 & \Omega_{12}\left[\cos(\omega_1 t) + \cos(\omega_2 t)\right] & E_{b2} \end{pmatrix}$$

For $\Omega_{01} \ll \Omega_{12} \ll |\Delta_1| \equiv |\omega_1 - E_{b1}/\hbar|$, which is analogous to the experimental conditions used here, we find that the two-photon resonance is shifted by

$$\frac{\hbar\Omega_{12}^2}{4\Delta_1} + \frac{\hbar\Omega_{12}^2}{4\left(\Delta_1 - E_{b2}/h\right)} \approx \frac{\hbar\Omega_{12}^2}{2\Delta_1}. \tag{4.16}$$

This agrees with our observation of a shift that is linear with intensity, and implies that the susceptibility is related to the Rabi frequency for a single-beam intensity I through $\chi_{689} \approx (\Omega_{12}/\sqrt{I})^2/(8\pi\Delta_1)$.

This single-resonance model [Eq. (4.16)] describes the observed shifts well for detuning close to the $\nu = -2$ state of the 0_u^+ molecular potential (small Δ_1). For large positive Δ_1, however, at which ω_1 and ω_2 approach atomic resonance, deviations indicate coupling to one or more other states (Fig. 4.6). The most likely suspects are the $\nu = -1$, $J = 1$ excited molecular state, bound by 1.633(1) MHz, and the ${}^1S_0 + {}^3P_1$ continuum. The sign of the deviation indicates that AC Stark shift of colliding ${}^1S_0$ atoms due to coupling to the ${}^3P_1$ state is dominant in this regime. We have neglected shifts due to collisions and the trapping laser, which are small at the large excitation-laser intensities used here.

A fit of the single-resonance model as shown in Fig. 4.6 yields $\Omega_{2,12}/2\pi \equiv \Omega_{12}/2\pi = 800\,\mathrm{kHz}$ for $I = 1\,\mathrm{W/cm^2}$. Note that $\Omega_{2,12}$ as defined here would be the splitting of the Autler-Townes doublet [10], which differs from the Bohn-Julienne

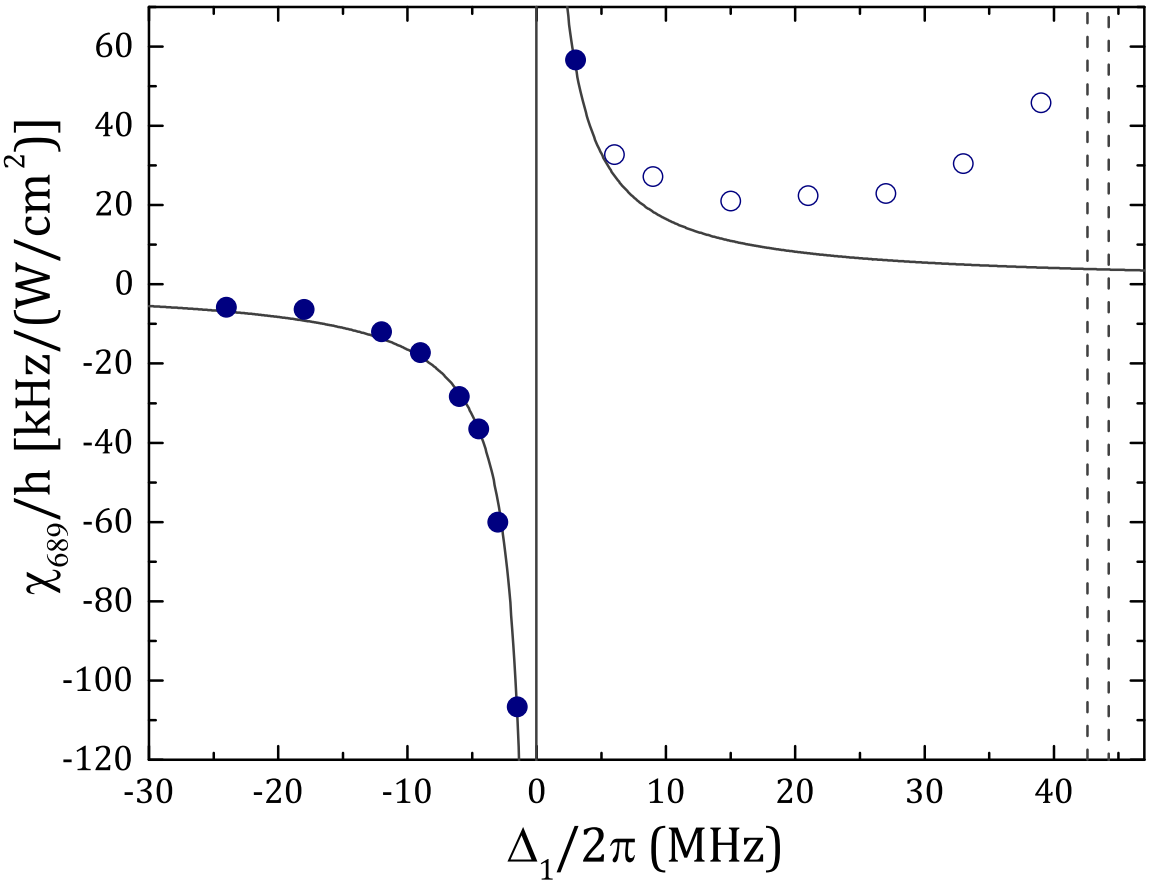

Figure 4.9 : Estimate of bound-bound coupling via isolated resonance model AC Stark shift susceptibility, χ_{689}. Dashed lines indicate the positions of the $\nu = -1$, $J = 1$ excited molecular state, bound by 1.633(1) MHz, and the $^1S_0$+$^3P_1$ continuum. Solid and open symbols show experimental measurements of the susceptibility. Using only the solid symbols, we fit a single resonance model of the form $\chi_{689} \approx (\Omega_{12}/\sqrt{I})^2/(8\pi\Delta_1)$ and show this fit result as a solid line.

definition of the molecular Rabi coupling [**?**]. From the measured $\Omega_{2,12}$, one can extract the Franck-Condon factor, f_{FCF}, reflecting the overlap of the ground and intermediate molecular states through

$$\Omega_{2,12} = \sqrt{f_{\mathrm{ROT}}}\sqrt{f_{\mathrm{FCF}}}\gamma_{\mathrm{atomic}}\sqrt{\frac{I}{2I_{\mathrm{sat,atom}}}} \tag{4.17}$$

where $I_{\mathrm{sat,atom}} = 2\pi^2\hbar c\gamma_{\mathrm{atomic}}/(3\lambda^3) = 3\,\mu\mathrm{W/cm}^2$ is the atomic saturation intensity for the ${}^1S_0$-${}^3P_1$ transition and $I = I_{689}/2$ is the single-beam intensity. The rotational factor f_{ROT} accounts for the change in dipole moment from atom to molecule due to symmetry of the wave function and projection on a rotating molecular axis. Following the formalism described in [10], $f_{\mathrm{ROT}} = 2$ for the $J = 1 \rightarrow 0$ bound-bound molecular transition studied here. This yields $f_{\mathrm{FCF}} = 0.03$.

From the formula for the line shape we can see that it depends on the spatial distribution of the atoms. The standard approximation made when measuring these types of systems is to ensure loss does not cause heating of the atoms during photoassociation. Heating results in re-equilibration of the atomic density distribition, which in turn effects the rate of loss creation. Without independent controls to keep the system in thermal (and therefore spatial density) equlibrium.

What are the things the rate equation deals with?

We need the desnity distribution.

In a harmonic trap, there if a simp[le anayltic form to the density distribution of a thermal gas. From Mi's work (and others) we know that this is only an approximation that is valid when eta is approx greater than 4. When greater than 4 we can apply the high-eta approx and the trap frequencies along a particular direction

reduce to ¡eq¿.

However, the trap we did this experiment in were at eta's of 1 or less so we don't have an analytic solution to the spatial distribution. Since this could be a problem we need to know what the trap looks like.

We measure trap oscillation freq. at several different powers and model the trap using the utility outlined somewhere else.

From the numeric model, we can define a spatially depedent eta which is determined by the local trap depth which is simply the difference between the local potential energy and the global depth. This is illustrated in fig something.

The spatial information is not only important for the density determination, but also for the range of available thermal energies. Consider two atoms near the local bottom of the trap. By definition, in equilibrium, a single atom may only have up to the trap depths worth of energy since any additional energy would result in its expulsion from the trap. In this case, in a relative momentum frame, the allowed collision energies range from zero to two times the trap depth. Similarly, as we move towards the edge of the trap the range of accessible collision energies shrinks. This additional weighting factor may be viewed as having a local truncasted Boltzmann ditribution at every point in space.

Normally the BZ dist goes to infinity but here we have a cutoff at 2 trap depeth. The most naive approx would be to simply consider the BZ and harshly truncate at 2 trap depth. We tried this

We know this is unphysical since we should expect that the probability of ob-

serving a certain momenta at a certain point in space, should smoothly tend zero towards as we approach the edge of the trap. To see what this looks like we (and determine how important the effect is) we rederive the relative momentum distribution.

¡Some stuff about center of mass and relative¿

What were all the cases and conclusions of having done this? Remember to consider what the different cases are. If the total relative energy can be X then how does that get split up? Use the plots to show this limiting behavior. Like if particle 1 has all the energy then there is only one possible value for particle 2 (and vice versa).

DERIVATION for truncated trap below

Need to lookup references for this molecular chaos assumption. What about egodicity? How to discuss that we may not be completely ergodic?

What does my potential look like? Can I make it a piecewise function? How should I introduce this part?

Where does the f equation come from? I believe this is just the normalized boltzmann factor for probability to occupy a particlar state.

We can truncate this single particle distribution by

$$f_{\mathbf{r}}(\mathbf{p}) = A\left(\frac{1}{2\pi k_B T}\right)^{3/2} e^{\left(\frac{-p^2}{2mk_BT}\right)} \Theta\left(\epsilon_{max} - U(\mathbf{r}) - \frac{p^2}{2m}\right) \tag{4.18}$$

where A is a normalization constant which ensures $\int_0^\infty f_{\mathbf{r}}(\mathbf{p})\, d\mathbf{p} = 1$ and $\Theta(x)$ is the Heaviside function defined by

$$\Theta(x) = \begin{cases} 1 & \text{if } x \geq 0, \\ 0 & \text{if } x < 0 \end{cases} \tag{4.19}$$

We got a certain answer with the way shown in the paper.

We can also use a completely different method that ignores all the consdierations of the last few sections. As was done in the calcium paper, we could simply fit the blue edge of the feature using a model function which can capture the high level features of the lineshape. Get the same answer. SHOW PLOTS TO THIS AFFECT AND COMPARE

Maybe go a little into the isolated resonance model (or at least recall), then tie into how we can measure the susceptibility across several different detunings which can give us the coupling to intermediate level. The first order analysis of this data suggest a bound-bound rabi freuqnecy of BLAH.

Point out the curling up at the end and say how the simple isolated resonacne model cannot predict. A full coupled channel calculation probably could but in the spirit of the Bohn and Julienne semi-classical approach, we set out to derive an approximate analytic expression to determine the binding energies. THis is presented in the next chapter.

Lastly, we note that in the context of photoassociation, the center-of-mass component of Eq.A.3 is not typically considered as typical PAS experiments are performed utilizing broad dipole allowed transitions which have linewidhts much greater than the doppler width thus only the relative momentum between particles is important

for determining the loss rate coefficeint K discussed in (somewhere).

The case of PA using narrow intercombination line transitions found in alkaline-earth-metal atoms

In general K is considered as a boltzmann average over a single loss rate constant This can be seen in [35] Eq. 1 where the loss rate constant is given by

$$\begin{aligned} K(\Delta, T) &= \langle \mathcal{K}(\Delta, \mathbf{P}_c, \mathbf{p}_r) \rangle \\ &= \int d^3\mathbf{P}_c \; f_M(\mathbf{P}_c) \int d^3\mathbf{p}_r \; f_\mu(\mathbf{p}_r) \; \mathcal{K}(\Delta, \mathbf{P}_c, \mathbf{p}_r) \end{aligned} \tag{4.20}$$

To this end we can integrate out the center of mass component to obtain the distribution most typically relevant to photoassociation.

By the time I've gotten to this I have already introduced K and that is not what I wanted to do.

conclusion here is the modified version of K we need for a trap that has a truncated energy disttribution

to get there normal version of K is given in ch3 this K can be given in terms of f? this ver4sion of f is given in the appendix why do I integrate out the com component?

typical PAS experiments utilize dipole allowed transitions which have linewidths many times larger than the

We now perform a change of variables using Eq. and Eq.A.2 can be rewritten as

Need to make a connection between dipole matrix element, wigner threshold, and infinite squarer step potential. This infiinite square step can be viewed as a dilute ideal gas.

To prove this assumption I want to show that using the square step I can get the same equations like in Eq. 1 of the 99 paper. Then once we know the infinite energy behavior (valid for only a particular portion of energy due to s-wave constraint) then we can ask what happens if f(p) is truncated.

In the s-wave limit I need to write K as a function of f(p) (should do this in the appendix proof and reference in body). Given the form of the loss rate constant K, our problem reduces to determining the form of f(p) when eta is finite.

Ok, so need to reference [35] to motivate usage of center of mass. Then use [36] Eq. 43 to reference the particular form

what is the throughline I want to make? Develop K_{in} $\rightarrow$ recast in terms of P distribution $\rightarrow$ show how we can replace the normal dist with a truncated dist $\rightarrow$ explore the effects of that truncation

Chapter 5

Strongly coupled PAS of a weakly bound molecule

5.1 Introduction

"Lorem ipsum dolor sit amet, consectetur adipiscing elit, sed do eiusmod tempor incididunt ut labore et dolore magna aliqua. Ut enim ad minim veniam, quis nostrud exercitation ullamco laboris nisi ut aliquip ex ea commodo consequat. Duis aute irure dolor in reprehenderit in voluptate velit esse cillum dolore eu fugiat nulla pariatur. Excepteur sint occaecat cupidatat non proident, sunt in culpa qui officia deserunt mollit anim id est laborum."

5.2 Experimental methods

"Lorem ipsum dolor sit amet, consectetur adipiscing elit, sed do eiusmod tempor incididunt ut labore et dolore magna aliqua. Ut enim ad minim veniam, quis nostrud exercitation ullamco laboris nisi ut aliquip ex ea commodo consequat. Duis aute irure dolor in reprehenderit in voluptate velit esse cillum dolore eu fugiat nulla pariatur. Excepteur sint occaecat cupidatat non proident, sunt in culpa qui officia deserunt mollit anim id est laborum."

5.3 Three level model

"Lorem ipsum dolor sit amet, consectetur adipiscing elit, sed do eiusmod tempor incididunt ut labore et dolore magna aliqua. Ut enim ad minim veniam, quis nostrud exercitation ullamco laboris nisi ut aliquip ex ea commodo consequat. Duis aute irure dolor in reprehenderit in voluptate velit esse cillum dolore eu fugiat nulla pariatur. Excepteur sint occaecat cupidatat non proident, sunt in culpa qui officia deserunt mollit anim id est laborum."

5.4 Resonance positions

"Lorem ipsum dolor sit amet, consectetur adipiscing elit, sed do eiusmod tempor incididunt ut labore et dolore magna aliqua. Ut enim ad minim veniam, quis nostrud exercitation ullamco laboris nisi ut aliquip ex ea commodo consequat. Duis aute irure dolor in reprehenderit in voluptate velit esse cillum dolore eu fugiat nulla pariatur. Excepteur sint occaecat cupidatat non proident, sunt in culpa qui officia deserunt mollit anim id est laborum."

5.5 Lineshape

"Lorem ipsum dolor sit amet, consectetur adipiscing elit, sed do eiusmod tempor incididunt ut labore et dolore magna aliqua. Ut enim ad minim veniam, quis nostrud exercitation ullamco laboris nisi ut aliquip ex ea commodo consequat. Duis aute irure dolor in reprehenderit in voluptate velit esse cillum dolore eu fugiat nulla pariatur. Excepteur sint occaecat cupidatat non proident, sunt in culpa qui officia deserunt mollit anim id est laborum."

5.6 Emergence of multi-photon Raman coupling

"Lorem ipsum dolor sit amet, consectetur adipiscing elit, sed do eiusmod tempor incididunt ut labore et dolore magna aliqua. Ut enim ad minim veniam, quis nostrud exercitation ullamco laboris nisi ut aliquip ex ea commodo consequat. Duis aute irure dolor in reprehenderit in voluptate velit esse cillum dolore eu fugiat nulla pariatur. Excepteur sint occaecat cupidatat non proident, sunt in culpa qui officia deserunt mollit anim id est laborum."

Chapter 6

Progress towards studies of quantum magnetism

A straightforward extension of the work presneted in this thesis would be to control interparticle spacing via an optical lattice. For these and additional experiments using quantum degenerate fermionic strontium we purchased and installed an optical lattice system. Our lattice is implemented using a Coherent Verdi V-18 which is shapped and propagated to our science chamber in free space. Fig shows the optical path for each arm of our cubic lattice.

Unfortunately, complications due to heating when loading the lattice has limited our success in this optical trap. I want to go over what we have been able to do so far with the lattice.

How did we characterize? Kaptiza-dirac extension

What convinced us we were having problems?

What are some ideas we could do in the lattice? Zeno faster cooling via stimulated raman potentailly? (can I model this somehow?) repulzively bound molecules? use interaction control in lattice with the zeno thing

6.1 $532\,nm$ optical lattice: installation and characterization

"Lorem ipsum dolor sit amet, consectetur adipiscing elit, sed do eiusmod tempor incididunt ut labore et dolore magna aliqua. Ut enim ad minim veniam, quis nostrud exercitation ullamco laboris nisi ut aliquip ex ea commodo consequat. Duis aute irure dolor in reprehenderit in voluptate velit esse cillum dolore eu fugiat nulla pariatur. Excepteur sint occaecat cupidatat non proident, sunt in culpa qui officia deserunt mollit anim id est laborum."

6.1.1 Background

This section should cover band structure and refer to the types of wavefunctions that are possible. Perhaps through some stuff in here from the quantum magnetism proposal from the NSF

6.1.2 Setup

This section should cover all the specifics regarding the lattice

6.1.3 Measurement and results

What are all the types of experiments we did in the lattice?

Cover sideband cooling and Bloch oscillations Results, look into why its not necessarily so easy from end of red MOT, thoughts on how it could become useful

Kaptiza-Dirac Scattering

Brief intro to theory and some plots showing fits.

Heating of a quantum degenerate gas

Creation of a Mott insulator and the results showing unacceptable heating rates

6.2 Spin manipulation of ^{87}Sr

Here is where I need to introduce and characterize the LCR

Averaging images together (how to use this code specifcally)

6.3 Search for narrowline PA molecules using various spin mixtures

"Lorem ipsum dolor sit amet, consectetur adipiscing elit, sed do eiusmod tempor incididunt ut labore et dolore magna aliqua. Ut enim ad minim veniam, quis nostrud exercitation ullamco laboris nisi ut aliquip ex ea commodo consequat. Duis aute irure dolor in reprehenderit in voluptate velit esse cillum dolore eu fugiat nulla pariatur. Excepteur sint occaecat cupidatat non proident, sunt in culpa qui officia deserunt mollit anim id est laborum."

Chapter 7

Conclusion

We have measured the binding energy of the least-bound vibrational level of the ground electronic state of the $^{86}Sr_2$ molecule with two-photon photoassociative spectroscopy. Using the universal prediction for the binding energy of a halo state including corrections derived for a van der Waals potential [Eq. (4.15)] [16, 17, 18], we extract an improved value of the s-wave scattering length.

We also characterized the AC Stark shift of the halo-state binding energy due to light near resonant with the single-photon photoassociation transition. A model only accounting for a single excited-state channel [**?**] cannot explain the observed frequency dependence of the AC Stark shift, which can be attributed to the proximity of other excited states.

Large AC Stark shifts of the halo state point to the possibility of optically tuning the ^{86}Sr scattering length, similar to recent demonstrations of optical tuning of magnetic Feshbach resonances [30, 12]. This is attractive because ground-state strontium lacks magnetic Feshbach resonances. With improved measurement of the photoassociation resonance frequency and its dependence on background atom density, perhaps combined with optical manipulation of the scattering length, it may also be possible to study the landscape of Efimov trimers associated with this naturally occurring scattering resonance. This work also points to the need for improved the-

ory, such as an improved calculation of the Sr ground-state molecular potential and C_6 coefficient, which could be compared with this high-accuracy measurement of the halo binding energy.

Bibliography

[1] J. A. Aman, J. C. Hill, R. Ding, K. R. A. Hazzard, T. C. Killian, and W. Y. Kon, "Photoassociative spectroscopy of a halo molecule in 86Sr," *Physical Review A*, vol. 98, p. 053441, nov 2018.

[2] L. B. Ratcliff, J. L. Fish, and D. D. Konowalow, "Electronic transition dipole moment functions for transitions among the twenty-six lowest-lying states of {L}i_2," *J. Mol. Spectrosc.*, vol. 122, p. 293, 1987.

[3] A. S. Jensen, K. Riisager, D. V. Fedorov, and E. Garrido, "Structure and reactions of quantum halos," *Reviews of Modern Physics*, vol. 76, no. 1, p. 215, 2004.

[4] T. Köhler, K. Góral, and P. S. Julienne, "Production of cold molecules via magnetically tunable {F}eshbach resonances," *Reviews of Modern Physics*, vol. 78, no. 4, p. 1311, 2006.

[5] E. Braaten and H. W. Hammer, "Universality in few-body systems with large scattering length," *Physics Reports*, vol. 428, p. 259, 2006.

[6] E. Braaten and H.-W. Hammer, "Efimov physics in cold atoms," *Annals of Physics*, vol. 322, p. 120, jan 2007.

[7] P. Naidon and S. Endo, "Efimov physics: A review," *Reports on Progress in Physics*, vol. 80, p. 56001, 2017.

[8] F. Luo, G. C. Mcbane, G. Kim, C. F. Giese, and W. R. Gentry, "The weakest bond: Experimental observation of helium dimer Effects of adiabatic, relativistic, and quantum electrodynamics interactions on the pair potential and thermophysical properties of helium The weakest bond: Experimental observation of helium dime," *The Journal of Chemical Physics The Journal of Chemical Physics The Journal of Chemical Physics*, vol. 981, no. 10, 1993.

[9] W. Scholikopf and J. P. Toennies, "Nondestructive Mass Selection of Small van der Waals Clusters," *Science*, vol. 266, no. 5189, p. 1345, 1994.

[10] E. Pachomow, V. P. Dahlke, E. Tiemann, F. Riehle, and U. Sterr, "Ground-state properties of Ca2 from narrow-line two-color photoassociation," *Physical Review A*, vol. 95, p. 043422, apr 2017.

[11] C. Chin and P. S. Julienne, "Radio-frequency transitions on weakly bound ultracold molecules," *Physical Review A - Atomic, Molecular, and Optical Physics*, vol. 71, no. 1, p. 12713, 2005.

[12] L. W. Clark, L. C. Ha, C. Y. Xu, and C. Chin, "Quantum Dynamics with Spatiotemporal Control of Interactions in a Stable Bose-Einstein Condensate," *Physical Review Letters*, vol. 115, p. 155301, 2015.

[13] N. R. Claussen, S. J. J. M. F. Kokkelmans, S. T. Thompson, E. A. Donley, E. Hodby, and C. E. Wieman, "Very-high-precision bound-state spectroscopy near a 85 Rb Feshbach resonance," *Physical Review A*, vol. 67, p. 60701, jun 2003.

[14] M. Greiner, C. A. Regal, and D. S. Jin, "Emergence of a molecular {B}ose-

{E}instein condensate from a {F}ermi gas," *Nature*, vol. 426, p. 537, 2003.

[15] S. Jochim, M. Bartenstein, A. Altmeyer, G. Hendl, S. Riedl, C. Chin, J. Hecker-Denschlag, and R. Grimm, "Bose-{E}instein condensation of molecules," *Science*, vol. 302, p. 2101, 2003.

[16] G. F. Gribakin and V. V. Flambaum, "Calculation of the scattering length in atomic collisions using the semiclassical approximation.pdf," *Physical Review A*, vol. 48, p. 546, jul 1993.

[17] B. Gao, "Angular-momentum-insensitive quantum-defect theory for diatomic systems," *Physical Review A - Atomic, Molecular, and Optical Physics*, vol. 64, p. 10701, 2001.

[18] B. Gao, "Binding energy and scattering length for diatomic systems," *Journal of Physics B: Atomic, Molecular and Optical Physics*, vol. 37, p. 4273, nov 2004.

[19] A. Stein, H. Knöckel, and E. Tiemann, "The $ˆ1$S+$ˆ1$S asymptote of {S}r$_2$ studied by Fourier-transform spectroscopy," *Eur. Phys. J. D*, vol. 57, p. 171, 2010.

[20] R. Ciurylo, E. Tiesinga, and P. S. Julienne, "Stationary phase approximation for the strength of optical {F}eshbach resonances," *Physical Review A*, vol. 74, p. 22710, 2006.

[21] M. Borkowski, A. A. Buchachenko, R. Ciuryło, P. S. Julienne, H. Yamada, Y. Kikuchi, K. Takahashi, Y. Takasu, and Y. Takahashi, "Beyond-Born-Oppenheimer effects in sub-kHz-precision photoassociation spectroscopy of ytterbium atoms," *Physical Review A*, vol. 96, p. 63405, 2017.

[22] R. Wynar, R. S. Freeland, D. J. Han, C. Ryu, and D. J. Heinzen, "Molecules in a {B}ose-{E}instein Condensate," *Science*, vol. 287, p. 1016, 2000.

[23] J. Wang, J. P. D'Incao, B. D. Esry, and C. H. Greene, "Origin of the Three-Body Parameter Universality in Efimov Physics," *Phys. Rev. Lett.*, vol. 108, p. 263001, 2012.

[24] X. Zhang, M. Bishof, S. L. Bromley, C. V. Kraus, M. S. Safronova, P. Zoller, A. M. Rey, and J. Ye, "Spectroscopic observation of SU(N) - symmetric interactions in Sr orbital magnetism," *Science*, vol. 345, p. 1467, aug 2014.

[25] P. M. A. Mestrom, J. Wang, C. H. Greene, and J. P. D'Incao, "Efimov-van der Waals universality for ultracold atoms with positive scattering lengths," *Physical Review A*, vol. 95, p. 32707, 2017.

[26] T. Köhler, T. Gasenzer, and K. Burnett, "Microscopic theory of atom-molecule oscillations in a Bose-Einstein condensate," *Physical Review A*, vol. 67, p. 13601, jan 2003.

[27] C. A. Regal, C. Ticknor, J. L. Bohn, and D. S. Jin, "Creation of ultracold molecules from a Fermi gas of atoms," *Nature*, vol. 424, p. 47, 2003.

[28] H. Moritz, T. Stoferle, K. Gunter, M. Kohl, and T. Esslinger, "Confinement Induced Molecules in a 1D Fermi Gas," *Physical Review Letters*, vol. 94, p. 210401, 2005.

[29] M. Bartenstein, A. Altmeyer, S. Riedl, R. Geursen, S. Jochim, C. Chin, J. H. Denschlag, R. Grimm, A. Simoni, E. Tiesinga, C. J. Williams, and P. S. Julienne, "Precise determination of6Li cold collision parameters by radio-frequency spec-

troscopy on weakly bound molecules," *Physical Review Letters*, vol. 94, no. 10, p. 103201, 2005.

[30] D. M. Bauer, M. Lettner, C. Vo, G. Rempe, and S. Durr, "Control of a magnetic {F}eshbach resonance with laser light," *Nature Physics*, vol. 5, p. 339, 2009.

[31] M. Theis, G. Thalhammer, K. Winkler, M. Hellwig, G. Ruff, R. Grimm, and J. H. Denschlag, "Tuning the Scattering Length with an Optically Induced Feshbach Resonance," *Physical Review Letters*, vol. 93, p. 123001, sep 2004.

[32] R. Yamazaki, S. Taie, S. Sugawa, and Y. Takahashi, "Submicron spatial modulation of an interatomic interaction in a bose-einstein condensate," *Physical Review Letters*, vol. 105, p. 050405, jul 2010.

[33] S. Blatt, T. L. Nicholson, B. J. Bloom, J. R. Williams, J. W. Thomsen, P. S. Julienne, and J. Ye, "Measurement of Optical Feshbach Resonances in an Ideal Gas," *Physical Review Letters*, vol. 107, p. 073202, aug 2011.

[34] M. Yan, B. J. DeSalvo, B. Ramachandhran, H. Pu, and T. C. Killian, "Controlling condensate collapse and expansion with an optical feshbach resonance," *Physical Review Letters*, vol. 110, p. 123201, mar 2013.

[35] R. Ciuryło, E. Tiesinga, S. Kotochigova, and P. S. Julienne, "Photoassociation spectroscopy of cold alkaline-earth-metal atoms near the intercombination line," *Physical Review A - Atomic, Molecular, and Optical Physics*, vol. 70, p. 062710, dec 2004.

[36] T. L. Nicholson, S. Blatt, B. J. Bloom, J. R. Williams, J. W. Thomsen, J. Ye, and P. S. Julienne, "Optical Feshbach resonances: Field-dressed theory and com-

parison with experiments," *Physical Review A - Atomic, Molecular, and Optical Physics*, vol. 92, p. 022709, aug 2015.

Appendices

Appendix A

Two-particle momentum probability distribution

A.1 Standard form

Typical derivation of relative momentum probability distribution function

We begin by considering the single particle momentum probability distritbuion function (gotten how)? Single particle momentum probability distribution

$$f^1(\mathbf{p}) = \left(\frac{1}{2\pi k_B T}\right)^{3/2} e^{\left(\frac{-p^2}{2mk_BT}\right)} \tag{A.1}$$

Extension of this simple Boltzmann equation into the two-particle regime is complicated due to dependence of each particle on the others. If however, we make the assumption that particle collisions are rapid (on some timescale) we can approximate the two particle momentum distribtuion as the product of two single particle functions. This is known as the moleculear chaos assumption and is important for what???

The two particle distribution for a homegeneous system is then

$$\begin{aligned} f^2(\mathbf{p}_1, \mathbf{p}_2) &= f^1(\mathbf{p}_1) f^1(\mathbf{p}_2) \\ &= \left(\frac{1}{2\pi m k_B T}\right)^3 \exp\left(\frac{-(p_1^2 + p_2^2)}{2mk_BT}\right) \end{aligned} \tag{A.2}$$

Next, we'd like to consider a center-of-mass frame for the distribution. So we'll define

we define the relative and center-of-mass momenta of the two particles by defining

$$\mathbf{P}_c = \mathbf{p}_1 + \mathbf{p}_2 \qquad M = m_1 + m_2 = 2m$$
$$\mathbf{p}_r = \frac{\mathbf{p}_1 - \mathbf{p}_2}{2} \qquad \mu = \frac{m_1 m_2}{m_1 + m_2} = \frac{m}{2}$$

from these equations we can use conservation of energy to determine the quadrature sum of the two momenta

$$\frac{p_1^2}{2m} + \frac{p_2^2}{2m} = \frac{P_c^2}{2M} + \frac{p_r^2}{2\mu}$$
$$p_1^2 + p_2^2 = \frac{P_c^2}{2} + 2p_r^2$$

thus the momentum probability distribution take the form

$$f^2(\mathbf{P}_c, \mathbf{p}_r) = \left(\frac{1}{2\pi M k_B T}\right)^{3/2} \left(\frac{1}{2\pi \mu k_B T}\right)^{3/2} \exp\left(\frac{-P_c^2}{2M k_B T}\right) \exp\left(\frac{-p_r^2}{2\mu k_B T}\right) \quad \text{(A.3)}$$

A.2 Truncated form

Here I will derive, motivate, and test limiting cases. Plots showing the effects of truncation will be in the main text

Two particle distribution (for correcting notation, use C and R when denoting

CoM and Rel)

$$f^2_{\mathbf{r},trunc}(\mathbf{p}_1,\mathbf{p}_2) = A^2\left(\frac{1}{2\pi m k_B T}\right)^3 \exp\left(\frac{-(p_1^2+p_2^2)}{2mk_BT}\right) \times \Theta\left(\epsilon_{max} - U(\mathbf{r}) - \frac{p_1^2}{2m}\right)\Theta\left(\epsilon_{max} - U(\mathbf{r}) - \frac{p_2^2}{2m}\right) \tag{A.4}$$

We have introduced a normalization constant A here to ensure the that integration over the truncated probability distribution remains equal to one.

The meaning of $_r$ is such that f should be evaluated at each point in space. Furthermore since the atoms are held in a trapping potential. each point in space has a local trap depth relative to the lip at the top of the trap need some figure to try and denote this

Want distribution of relative momenta so integrate out center of mass. Going to drop the two and trunc for now

$$\begin{aligned}\tilde{f}_{\mathbf{r}}(\mathbf{p}_{rel}) &= \int d^3\mathbf{P}_c\, f_{\mathbf{r}}(\mathbf{p}_1,\mathbf{p}_2) \\ &= \left(\frac{1}{2\pi M k_B T}\right)^{3/2}\left(\frac{1}{2\pi \mu k_B T}\right)^{3/2} A^2 \int d^3\mathbf{P}_c\, e^{\left(\frac{-P_c^2}{2Mk_BT}\right)} e^{\left(\frac{-p_r^2}{2\mu k_B T}\right)} \\ &\quad\times\ \Theta\left(\epsilon_{max} - U(\mathbf{r}) - \frac{P_c^2}{8m} - \frac{p^2}{2m} - \frac{\mathbf{P}_c\cdot\mathbf{p}}{2m}\right)\Theta\left(\epsilon_{max} - U(\mathbf{r}) - \frac{P_c^2}{8m} - \frac{p^2}{2m} + \frac{\mathbf{P}_c\cdot\mathbf{p}}{2m}\right)\end{aligned} \tag{A.5}$$

Spherically symetrix collisions so can integrate by transforming into spherical coordinates with the radius aligned along the interatomic axis

$$\begin{aligned}\tilde{f}_{\mathbf{r}}(\mathbf{p}) &= \left(\frac{1}{2\pi M k_B T}\right)^{3/2}\left(\frac{1}{2\pi \mu k_B T}\right)^{3/2} e^{\left(\frac{-p_r^2}{2\mu k_B T}\right)} A^2 \int_0^{\pi}\sin\theta d\theta \int_0^{2\pi} d\phi \int_0^{\infty} dP_c\, P_c^2\, e^{\left(\frac{-P_c^2}{2Mk_BT}\right)} \\ &\quad\times\ \Theta\left(\epsilon_{max} - U(\mathbf{r}) - \frac{P_c^2}{8m} - \frac{p^2}{2m} - \frac{P_c\, p\cos\theta}{2m}\right)\Theta\left(\epsilon_{max} - U(\mathbf{r}) - \frac{P_c^2}{8m} - \frac{p^2}{2m} + \frac{P_c\, p\cos\theta}{2m}\right)\end{aligned} \tag{A.6}$$

$$X = \cos\theta$$

$$dX = -\sin\theta d\theta$$

Substitute and integrate over ϕ

$$\tilde{f}_{\mathbf{r}}(\mathbf{p}) = \left(\frac{1}{2\pi M k_B T}\right)^{3/2}\left(\frac{1}{2\pi\mu k_B T}\right)^{3/2} e^{\left(\frac{-p_r^2}{2\mu k_B T}\right)} 2\pi A^2 \int_{-1}^{1} dX \int_0^{\infty} dP_c\, P_c^2\, e^{\left(\frac{-P_c^2}{2M k_B T}\right)} \times\ \Theta\left(\epsilon_{max} - U(\mathbf{r}) - \frac{P_c^2}{8m} - \frac{p^2}{2m} - \frac{P_c\, pX}{2m}\right)\Theta\left(\epsilon_{max} - U(\mathbf{r}) - \frac{P_c^2}{8m} - \frac{p^2}{2m} + \frac{P_c\, pX}{2m}\right) \tag{A.7}$$

Recognize that the Heaviside functions cancel each other out on either side of zero, so can eliminate one of the Heavisides and multiply by 2

$$\tilde{f}_{\mathbf{r}}(\mathbf{p}) = \left(\frac{1}{2\pi M k_B T}\right)^{3/2}\left(\frac{1}{2\pi\mu k_B T}\right)^{3/2} e^{\left(\frac{-p_r^2}{2\mu k_B T}\right)} 4\pi A^2 \int_{0}^{1} dX \int_0^{\infty} dP_c\, P_c^2\, e^{\left(\frac{-P_c^2}{2M k_B T}\right)} \times\ \Theta\left(\epsilon_{max} - U(\mathbf{r}) - \frac{P_c^2}{8m} - \frac{p^2}{2m} - \frac{P_c\, pX}{2m}\right) \tag{A.8}$$

From here we can rewrite using the infinite relative momentum probability distribution $f_{\mathbf{r},\infty}(\mathbf{p})$ from some equation

$$\begin{aligned}\tilde{f}_{\mathbf{r}}(\mathbf{p}) &= \left(\frac{1}{2\pi\mu k_B T}\right)^{3/2} e^{\left(\frac{-p_r^2}{2\mu k_B T}\right)}\mathcal{G}(T, \epsilon_{max}, p_{rel}) \\ &= f_{\mathbf{r},\infty}(\mathbf{p})\mathcal{G}(T, \epsilon_{max}, p_{rel})\end{aligned} \tag{A.9}$$

where $\mathcal{G}(T, \epsilon_{max}, p_{rel})$ is given by

$$\mathcal{G}(T,\epsilon_{max},p_{rel}) = A^2\left(\frac{4\pi}{2\pi M k_B T}\right)^{3/2}\int_0^1 dX\int_0^\infty dP_c\, P_c^2\, e^{\left(\frac{-P_c^2}{2Mk_BT}\right)} \times\ \Theta\left(\epsilon_{max} - U(\mathbf{r}) - \frac{P_c^2}{8m} - \frac{p^2}{2m} - \frac{P_c\, pX}{2m}\right) \tag{A.10}$$

Now define two dimensionless variables $\tilde{\epsilon}$ and $\tilde{E}$ which will be used to change variables once more

$$\tilde{\epsilon} = \frac{p_{rel}^2}{2\mu k_B T} \qquad \tilde{E} = \frac{P_c^2}{2Mk_BT}$$
$$p = \sqrt{2\mu k_B T\tilde{\epsilon}} \qquad P_c = \sqrt{2Mk_BT\tilde{E}}$$
$$dpp^2 = \frac{\sqrt{\tilde{\epsilon}}}{2}(2\mu k_B T)^{3/2}d\tilde{\epsilon} \qquad dP_c\, P_c^2 = \frac{\sqrt{\tilde{E}}}{2}(2Mk_BT)^{3/2}d\tilde{E}$$

Plugging these expressions into Eq.A.10 and rearranging

$$\tilde{f}_{\mathbf{r}}(\mathbf{p}) = A^2\frac{e^{-\tilde{\epsilon}}}{(2\pi\mu k_B T)^{3/2}}\int_0^1 dX\frac{2}{\sqrt{\pi}}\int_0^\infty d\tilde{E}e^{-\tilde{E}}\sqrt{\tilde{E}} \times\Theta\left(\eta(\mathbf{r}) - \frac{\tilde{E}}{2} - \frac{\tilde{\epsilon}}{2} - X\sqrt{\tilde{E}\tilde{\epsilon}}\right) \tag{A.11}$$

would like to turn this distribution into a relative energy distrbution. Collisions are isotropic so we can use the relation

$$\int dpp^2\int d\Omega_p\tilde{f}_{\mathbf{r}}(\mathbf{p}) = \int d\tilde{\epsilon}\hat{f}_{\mathbf{r}}(\tilde{\epsilon})) = 1 \Rightarrow 4\pi p^2\tilde{f}_{\mathbf{r}}(\mathbf{p})dp = \hat{f}_{\mathbf{r}}(\tilde{\epsilon})d\tilde{\epsilon} \tag{A.12}$$

using dpp^2 given above we then write

$$\hat{f}_{\mathbf{r}}(\tilde{\epsilon}) = A^2\sqrt{\tilde{\epsilon}}\, e^{-\tilde{\epsilon}}\frac{2}{\sqrt{\pi}}\int_0^1 dX \frac{2}{\sqrt{\pi}}\int_0^\infty d\tilde{E} e^{-\tilde{E}}\sqrt{\tilde{E}}\;\Theta\left(\eta(\mathbf{r}) - \frac{\tilde{E}}{2} - \frac{\tilde{\epsilon}}{2} - X\sqrt{\tilde{E}\tilde{\epsilon}}\right) \tag{A.13}$$

We can now choose the normalization constant A^2 using

$$\int_0^{2\eta(\mathbf{r})} d\tilde{\epsilon}\hat{f}_{\mathbf{r}}(\tilde{\epsilon}) = 1$$

where we have used an energy cutoff of $2\eta(\mathbf{r})$ since either particle may have an energy in the range $[0 \to \eta(\mathbf{r})]$. With the normalization, the complete expression for $\hat{f}_{\mathbf{r}}(\tilde{\epsilon})$ is then

$$\hat{f}_{\mathbf{r}}(\tilde{\epsilon}) = \frac{2}{\sqrt{\pi}}\sqrt{\tilde{\epsilon}}\, e^{-\tilde{\epsilon}}\hat{\mathcal{G}}(\eta_{\mathbf{r}}, \tilde{\epsilon}) \tag{A.14}$$

where all the effects of the truncation have been moved to $\hat{\mathcal{G}}$, given by

$$\hat{\mathcal{G}}(\eta_{\mathbf{r}}, \tilde{\epsilon}) = \frac{\displaystyle\int_0^1 dX \frac{2}{\sqrt{\pi}}\int_0^\infty d\tilde{E} e^{-\tilde{E}}\sqrt{\tilde{E}}\;\Theta\left(\eta(\mathbf{r}) - \frac{\tilde{E}}{2} - \frac{\tilde{\epsilon}}{2} - X\sqrt{\tilde{E}\tilde{\epsilon}}\right)}{\displaystyle\int_0^{2\eta(\mathbf{r})} d\tilde{\epsilon}\frac{2}{\sqrt{\pi}}\sqrt{\tilde{\epsilon}}\, e^{-\tilde{\epsilon}}\int_0^1 dX \frac{2}{\sqrt{\pi}}\int_0^\infty d\tilde{E} e^{-\tilde{E}}\sqrt{\tilde{E}}\;\Theta\left(\eta(\mathbf{r}) - \frac{\tilde{E}}{2} - \frac{\tilde{\epsilon}}{2} - X\sqrt{\tilde{E}\tilde{\epsilon}}\right)}$$

we can check the limiting behavior of this equation since we expect when

$$\lim_{\eta\to\infty}\hat{\mathcal{G}}(\eta_{\mathbf{r}}, \tilde{\epsilon}) = 1$$

. Indeed, remembering that

$$\int_0^\infty dx\sqrt{x}e^{-x} = \frac{\sqrt{\pi}}{2}$$

then this requirement is fulfilled.

Appendix B

Imagefit analysis routine

"Lorem ipsum dolor sit amet, consectetur adipiscing elit, sed do eiusmod tempor incididunt ut labore et dolore magna aliqua. Ut enim ad minim veniam, quis nostrud exercitation ullamco laboris nisi ut aliquip ex ea commodo consequat. Duis aute irure dolor in reprehenderit in voluptate velit esse cillum dolore eu fugiat nulla pariatur. Excepteur sint occaecat cupidatat non proident, sunt in culpa qui officia deserunt mollit anim id est laborum."

B.1 Background removal

Would like to remove noisy fringes to fit more easily

B.1.1 Principal component analysis

B.2 Fitting the spatial distribution

B.3 Evaluating fit parameters

B.3.1 How to write a new plugin

Appendix C

neuKLEIN - Killian lab experimental interface

During my time working on the neutral apparatus, Joe Whalen began a rewrite of the Labview based experimental control software which had grown organically through the first decade of the neutral apparatus' existence. Following this refactor, the user interface was also revamped to help reduce human errors and improve overall data collection efficiency. This chapter will outline the major components of the neuKLEIN software package and how this system integrates with the hardware control system and the software analysis algorithm.

C.1 Labview code

Need to have description of state machine.

Need to

Use of references for updating front panel

Need to get references for LV documentation for this stuff

Discuss triggered waveform oddity (retriggerable setup)

C.2 FPGA code

The versatility of FPGA led us to want to simple system for setting static voltages and switching them at will. We built such a system using an National Instrument FPGA device (Xlinix something). The hardware details and circuitry are available in appendix blah. This section will focus on the software side of programming and using the FPGA system.

This was originally a project started by a summer student named Weixuan Li in summer 2018. He did a good job.

Talk about special programs (the custom operation builder specifically)

C.3 Possible future improvements

Specifically thinking about the ability to do network shared variables. Then we could dedicate a mahcine to an instrument and share the data using a networking layer instead of a hard connection.

Movement to full state machine

Standardization of the triggered waveform VI

implementation of coupled scanning mechanism (how is this currently handled)

Appendix D

Experimental control computer hardware

"Lorem ipsum dolor sit amet, consectetur adipiscing elit, sed do eiusmod tempor incididunt ut labore et dolore magna aliqua. Ut enim ad minim veniam, quis nostrud exercitation ullamco laboris nisi ut aliquip ex ea commodo consequat. Duis aute irure dolor in reprehenderit in voluptate velit esse cillum dolore eu fugiat nulla pariatur. Excepteur sint occaecat cupidatat non proident, sunt in culpa qui officia deserunt mollit anim id est laborum."

D.1 Overview of status

D.2 Migration to a new machine

Appendix E

Concise derivation of effective volumes

The following derivation is meant to serve as a quick reference for finding the analytic form of the effective volumes for ultracold gases held in a optical dipole trap. This section follows the arguements presented by Mi's paper which considers and numerically evalutes the general case of power-law potentials and the corresponding ddensity distribution at arbitrary temperatures less than the trap depth.

If instead one restricts to the experimentally reasonable conditions of high-η (recall η is the ratio of trap depth to sample temperature, $\eta = \epsilon_t / k_B T$) and harmonic trapping potentials, then a useful analytic expression can be found for the effective volumes of the gas.

Following eff volume derivation from first year

Appendix F

Repair of 922 Lynx master

"Lorem ipsum dolor sit amet, consectetur adipiscing elit, sed do eiusmod tempor incididunt ut labore et dolore magna aliqua. Ut enim ad minim veniam, quis nostrud exercitation ullamco laboris nisi ut aliquip ex ea commodo consequat. Duis aute irure dolor in reprehenderit in voluptate velit esse cillum dolore eu fugiat nulla pariatur. Excepteur sint occaecat cupidatat non proident, sunt in culpa qui officia deserunt mollit anim id est laborum."

Appendix G

Custom circuitry

"Lorem ipsum dolor sit amet, consectetur adipiscing elit, sed do eiusmod tempor incididunt ut labore et dolore magna aliqua. Ut enim ad minim veniam, quis nostrud exercitation ullamco laboris nisi ut aliquip ex ea commodo consequat. Duis aute irure dolor in reprehenderit in voluptate velit esse cillum dolore eu fugiat nulla pariatur. Excepteur sint occaecat cupidatat non proident, sunt in culpa qui officia deserunt mollit anim id est laborum."

G.1 AC line zero crossing trigger

G.2 Hard drive shutters

G.3 Power locks

G.4 Photodiodes

G.5 Infinite sample and hold

G.5.1 Reduced intensity fluctuations for sub-hertz exposures

Don't forget to talk about whatever noise I observed. I think there is a picture on my phone of this.

Appendix H

Miscellaneous tips and tricks

"Lorem ipsum dolor sit amet, consectetur adipiscing elit, sed do eiusmod tempor incididunt ut labore et dolore magna aliqua. Ut enim ad minim veniam, quis nostrud exercitation ullamco laboris nisi ut aliquip ex ea commodo consequat. Duis aute irure dolor in reprehenderit in voluptate velit esse cillum dolore eu fugiat nulla pariatur. Excepteur sint occaecat cupidatat non proident, sunt in culpa qui officia deserunt mollit anim id est laborum."

H.1 Alignment of GHz AOM

H.2 Using the Picoscope in Labview(TM)

H.3 Liquid crystal retarder

H.4 Newport(TM) optomotion control

H.5 Fast analog lock for 689 nm

H.6 Porta CoM technique

H.7 Measuring Rabi frequencies